FER-LIKE IRON DEFICIENCY-INDUCED TRANSCRIPTION FACTOR (FIT) accumulates in homo- and heterodimeric complexes in dynamic and inducible nuclear condensates associated with speckle components

Short title: FIT localizes in condensates

Ksenia Trofimov[1], Regina Gratz[1,§], Rumen Ivanov[1], Yvonne Stahl[2,3], Petra Bauer[1,3,*], Tzvetina Brumbarova[1,*]

[1] Institute of Botany, Heinrich-Heine-University, 40225 Düsseldorf, Germany
[2] Institute for Developmental Genetics, Heinrich-Heine-University, 40225 Düsseldorf, Germany
[3] Cluster of Excellence on Plant Science (CEPLAS), Heinrich-Heine-University, 40225 Düsseldorf, Germany
***** Shared corresponding authors: Tzvetina Brumbarova (Tzvetina.Brumbarova@hhu.de), Petra Bauer (Petra.Bauer@hhu.de)
[§] Present address: Department of Forest Genetics and Plant Physiology, Swedish University of Agricultural Sciences, 90183 Umeå, Sweden

The author responsible for distribution of materials integral to the findings presented in this article in accordance with the policy described in the Instructions for Authors (https://academic.oup.com/plcell/pages/General-Instructions) is: Petra Bauer (Petra.Bauer@hhu.de).

Highlights

- FIT undergoes light-induced, reversible condensation and localizes to nuclear bodies (NBs), likely via liquid-liquid phase separation
- Functionally relevant Ser271/272 defines an intrinsically disordered region and influences NB formation dynamics
- NBs are preferential sites for FIT dimerization with FIT and bHLH039, dependent on Ser271/272
- FIT NBs colocalize with NB markers related to splicing and light signaling
- Light conditions inducing NBs are linked with active FIT, in agreement with elevated FIT target gene expression in roots

Keywords

bHLH039, condensates, FIT, FRET, intrinsically disordered region, blue light, liquid-liquid phase separation, nuclear body, speckle, SR45

33 **Abbreviations**

34 bHLH	basic helix-loop-helix
35 bHLH039	BASIC HELIX-LOOP-HELIX039
36 C	mCherry
37 FIT	FER-LIKE IRON DEFICIENCY-INDUCED TRANSCRIPTION FACTOR
38 FLIM	fluorescence lifetime imaging microscopy
39 FRAP	fluorescence recovery after photobleaching
40 FRET	fluorescence resonance energy transfer
41 G	GFP
42 GFP	GREEN FLUORESCENT PROTEIN
43 IDR	intrinsically disordered region
44 IR	intron retention
45 LLPS	liquid-liquid phase separation
46 mCherry	monomeric Cherry
47 mRFP	monomeric RED FLUORESCENT PROTEIN
48 NB	nuclear body
49 NP	nucleoplasm
50 PB	photobody
51 R	mRFP
52 TF	transcription factor

Abstract

Some nuclear proteins undergo condensation, but the functional importance remains often unclear. The basic helix-loop-helix (bHLH) FER-LIKE IRON DEFICIENCY-INDUCED TRANSCRIPTION FACTOR (FIT) integrates internal and external signals to control iron acquisition and growth. The previously described C-terminal residues Ser271/272 allow FIT to form active complexes with subgroup Ib bHLH factors such as bHLH039. FIT has lower nuclear mobility than mutant FITmSS271AA. Here, we show that FIT undergoes a light-inducible subnuclear partitioning into nuclear condensates that we termed FIT nuclear bodies (NBs). FIT NB characteristics were examined using a standardized FIT NB analysis procedure coupled with different types of quantitative and qualitative microscopy-based approaches. FIT condensates were reversible and likely formed by liquid-liquid phase separation. FIT accumulated preferentially in FIT NBs versus nucleoplasm when engaged in protein complexes with itself and with bHLH039. FITmSS271AA, instead, localized to NBs with different dynamics. FIT colocalized with splicing and light signaling NB markers. The NB-inducing light conditions were linked with active FIT and elevated FIT target gene expression in roots. Hence, we conclude that inducible, highly dynamic FIT condensates form preferentially when transcription factor complexes are active. Inducible FIT nuclear condensates may affect nuclear mobility and integrate environmental and Fe nutrition signals.

72 **Introduction**

73 As sessile organisms, plants adjust to an ever-changing environment and acclimate
74 rapidly. They also control the amount of micronutrients they take up. Even though iron is
75 one of the most abundant elements in the soil, its bioavailability as micronutrient is limited
76 in most soils (Römheld and Marschner, 1986; Wedepohl, 1995). This poses a particular
77 challenge for plants as they need mobilizing iron while at the same time must prevent that
78 iron over-accumulates and becomes toxic in cells.

79 An essential regulatory protein needed for iron acquisition is the basic helix-loop-
80 helix (bHLH) transcription factor (TF) FER-LIKE IRON DEFICIENCY-INDUCED
81 TRANSCRIPTION FACTOR (FIT; Colangelo and Guerinot, 2004; Jakoby et al., 2004;
82 Yuan et al., 2005; Bauer et al., 2007). FIT is activated upon iron deficiency downstream
83 of a cascade of bHLH TFs (Zhang et al., 2015; Li et al., 2016b; Liang et al., 2017; Kim et
84 al., 2019; Gao et al., 2020) and of a calcium-sensing protein kinase able to target
85 phosphorylation site Ser271/272 of FIT (Gratz et al., 2019). FIT alone is not sufficient to
86 upregulate iron acquisition, while it is active in a heterodimeric complex together with a
87 member of the bHLH subgroup Ib such as bHLH039 (Yuan et al., 2008; Wang et al., 2013).
88 Furthermore, FIT action is regulated through protein-protein contacts with multiple key
89 players of hormonal and abiotic stress signaling pathways (Lingam et al., 2011; Le et al.,
90 2016; Wild et al., 2016; Cui et al., 2018; Gratz et al., 2019, 2020). Thus, FIT behaves as
91 a regulatory hub in root cells that perceives external and internal cues to adjust iron
92 acquisition with growth (Schwarz and Bauer, 2020; Kanwar et al., 2021).

93 The subcellular localization of the FIT-bHLH039 module is remarkable. bHLH039
94 alone is inactive and present mainly close to the plasma membrane in cytoplasmic foci,
95 while bHLH039 together with FIT localizes in the nucleus (Trofimov et al., 2019). FIT is
96 predominately localized in the nucleus but not as mobile compared to mutant
97 FITmSS271AA, that is a less active mutant form of FIT (Gratz et al., 2019). Subcellular
98 partitioning of proteins involved in nutrient uptake has until now not been enough in the
99 focus of research to understand the significance of differing subcellular localization
100 patterns.

101 One prominent type of subnuclear partitioning occurs when biomolecular
102 condensates, or nuclear bodies (NBs), form. NBs are membrane-less, nuclear sub-
103 compartments, which can be of stable or dynamic nature. To form condensates, proteins
104 need to have particular features that enable protein interactions and compaction in three-

105 dimensional space. Intrinsically disordered regions (IDRs) are flexible protein regions that
106 allow conformational changes, and thus various interactions, leading to the required
107 multivalency of a protein for condensate formation (Tarczewska and Greb-Markiewicz,
108 2019; Emenecker et al., 2020). As Arabidopsis TFs are enriched in IDRs (Strader et al.,
109 2022) it is not unlikely that the resulting multivalency in TFs drives condensation and
110 results in microenvironments for interaction, probably more often than so far studied. IDRs
111 are particularly characteristic in bHLH TFs in vertebrates and invertebrates (Tarczewska
112 and Greb-Markiewicz, 2019), suggesting that this feature may also be relevant for the
113 bHLH TFs of plants. One possibility for condensates to form is to undergo liquid-liquid
114 phase separation (LLPS). In this process, a solution is demixed into two or more phases
115 (Emenecker et al., 2020). This mechanism has been examined in simplified *in vitro*
116 systems, but the involvement of different cell components renders the mechanism more
117 complex *in vivo* (Fang et al., 2019; Riback et al., 2020; Zhu et al., 2021).
118 Various NBs are found. Plants and animals share several of them, e.g. the
119 nucleolus, Cajal bodies, and speckles. The nucleolus is involved in transcription of
120 ribosomal DNA, processing of ribosomal RNA, and ribosome biogenesis (Kalinina et al.,
121 2018; Lafontaine et al., 2021). Nucleoli share components and function with Cajal bodies,
122 which are e.g. ribonucleoproteins and RNA processing (Love et al., 2017; Trinkle-Mulcahy
123 and Sleeman, 2017). Speckles are known spliceosomal sites (Reddy et al., 2012;
124 Galganski et al., 2017). Plant-specific NBs are photobodies (PBs), which are triggered by
125 light, temperature, and circadian clock (Pardi and Nusinow, 2021). PBs harbor regulatory
126 complexes of the photomorphogenic responses, including photoreceptors like
127 phytochromes (phy) and bHLH TFs belonging to the PHYTOCHROME INTERACTING
128 FACTORs (PIFs; Pardi and Nusinow, 2021). Another trigger for inducible and reversible
129 condensate formation is temperature (Jung et al., 2020; Zhu et al., 2021).
130 NBs may act as hubs integrating environmental signals (Emenecker et al., 2020;
131 Meyer, 2020). Especially PBs may combine external cues, such as light, as an input signal
132 to steer developmental processes (Kaiserli et al., 2015; Meyer, 2020; Pardi and Nusinow,
133 2021). It is proposed that the formation of NBs could be an ancient mechanism for spatial
134 organization within the nucleus (Emenecker et al., 2020). As more evidence on
135 condensation in plants arises, this topic remains barely examined in the scope of plant
136 nutrition.

137 Here, we report a novel property of FIT, namely that FIT undergoes light-inducible
138 and reversible nuclear condensation, which we detected as FIT nuclear bodies (NBs). The
139 motivation for our study was then to elucidate the mechanism behind subcellular
140 distribution and nuclear mobility of FIT and obtain functional hints. We developed a
141 standardized FIT NB analysis procedure to characterize quantitative and qualitative
142 aspects of the dynamic NB formation using different microscopy-based techniques.
143 Thereby, we linked FIT NB formation with the activity status of FIT to form functional
144 protein complexes. Splicing was also associated with the light-induced FIT NBs. Thus,
145 this study suggests that FIT NBs are regulatory hubs steering nutritional signalling, and
146 associating functional significance to FIT protein condensate formation.

147 **Results**

148 **FIT localizes to NBs in light-inducible and dynamic manner likely as a result of LLPS**

149 The TF FIT has a dynamic mobility and capacity to form TF complexes inside plant
150 cells (Gratz et al., 2019; Trofimov et al., 2019). To explore possible mechanisms for
151 dynamic FIT subcellular localization, we performed a microscopic study on FIT-GFP
152 protein localization in the root epidermis of the root differentiation zone of 5-d-old iron-
153 deficient seedlings of *Arabidopsis thaliana* (Arabidopsis), where FIT is active and iron
154 acquisition occurs (FIT_{pro}:FIT-GFP, this study; $35S_{pro}$:FIT-GFP, Gratz et al., 2019). At first
155 microscopic inspection, FIT-GFP was evenly distributed within the nucleus (t= 0 in
156 **Figure 1A**, FIT_{pro}:FIT-GFP; t= 0 in **Supplemental Figure S1A**, $35S_{pro}$:FIT-GFP), as
157 expected (Gratz et al., 2019; Trofimov et al., 2019). When whole seedlings were exposed
158 to 488 nm laser light for several minutes, FIT became re-localized at the subnuclear level.
159 After a lag time, FIT-GFP was present in one to four discrete spots per nucleus, visible
160 after 40 min earliest, sometimes taking up to 120 min to appear (t= 90 minutes in
161 **Figure 1A**, FIT_{pro}:FIT-GFP; t= 40 min in **Supplemental Figure S1A**, $35S_{pro}$:FIT-GFP).
162 Hence, FIT-GFP was re-localized in a blue light-inducible manner at the subnuclear level,
163 irrespective of either of the two promoters used. During the imaging process or an
164 additional hour of darkness, these spots disappeared (**Figure 1A**, t= 120 min), indicating
165 that the formation of these spots was reversible. Seedlings that were kept in white light
166 and imaged immediately did not show this localization pattern (**Supplemental**
167 **Figure S1B)**. The observation of FIT nuclear spots in the root epidermis of the root
168 differentiation zone was very interesting, suggesting that these might perhaps be NBs

169 containing FIT. However, further inspection of the nuclear spots in root cells in this
170 differentiating root zone was challenged by the small size and low accessibility of the
171 nucleus, and especially considering the long lag time for detecting the nuclear spots.
172 These factors made it impossible for us to apply quantitative fluorescence microscopy
173 techniques to draw validated conclusions on the nature, dynamics, and functional
174 significance of nuclear spots in root epidermis cells of the root differentiation zone of iron-
175 deficient seedlings.

176 Since we had previously established a reliable plant cell assay for studying FIT
177 functionality, we adapted it to study the characteristics of the prospective FIT NBs (Gratz
178 et al., 2019, 2020; Trofimov et al., 2019). For this assay, FIT-GFP was transiently
179 expressed in *Nicotiana benthamiana* (*N. benthamiana*) leaf epidermis cells under a β-
180 estradiol-inducible promoter. Under such controlled protein expression condition, FIT-
181 GFP re-localized also into nuclear spots as observed in the Arabidopsis root epidermis,
182 again triggered by treatment with a 488 nm laser light stimulus. Differences were,
183 however, the duration of the lag time needed to observe this phenomenon, and the
184 number of nuclear spots. As in Arabidopsis, FIT-GFP localized initially in uniform manner
185 to the entire nucleus (t=0) of *N. benthamiana* leaf epidermis cells (**Figure 1B**). A short
186 duration of 1 min 488 nm laser light excitation induced the formation of FIT-GFP signals
187 in discrete spots inside the nucleus, which became fully visible after only five minutes (t=5;
188 **Figure 1B and Supplemental Movie S1A**). The nuclear FIT spots were systematically
189 initiated, and nearly all nuclei in the imaged leaf disk showed numerous spots. A similar
190 laser light excitation procedure was previously found to elicit PB formation of
191 cryptochrome2 (CRY2) in Arabidopsis protoplasts and HEK293T cells (Wang et al., 2021).
192 We deduced that the spots of FIT-GFP signal were indeed very likely NBs (for this reason
193 hereafter termed FIT NBs). FIT NB formation was not dependent on the fluorescent tag,
194 as it was similar for FIT-mCherry when co-excited with 488 nm laser light (**Figure 1C**).
195 Another TF and interactor of FIT, ZINC FINGER OF ARABIDOPSIS THALIANA12-GFP
196 (ZAT12-GFP; Le et al., 2016), did not localize to NBs under the same imaging conditions
197 (**Figure 1D and Supplemental Movie S1B**). Therefore, we concluded that FIT
198 localization to NBs was a specificity of FIT and that formation of FIT NBs was not artificially
199 caused by fluorescent tags or the imaging setup. Importantly, the *N. benthamiana*
200 epidermis expression system was suited to control the parameters for light-induced
201 triggering of FIT NBs and their quantitative analysis by fluorescence microscopy. We then

202 developed a standardized experimental procedure for qualitative and quantitative FIT NB
203 analysis in *N. benthamiana* (hereafter named 'standardized FIT NB analysis procedure';
204 **Supplemental Figure S1C**).
205 Liquid-liquid phase separation (LLPS) is a possible way for condensate formation,
206 and liquid-like features are quantifiable by mobility and shape analysis within condensates
207 (Shin et al., 2017; Wang et al., 2021). We used the standardized FIT NB analysis
208 procedure to examine whether this could also be a mechanism underlying the FIT NB
209 formation. Mobility of FIT NBs was tested with the fluorescence recovery after
210 photobleaching (FRAP) approach (Bancaud et al., 2010; Trofimov et al., 2019) by
211 recording the recovery of the fluorescence intensity over time in a bleached NB
212 (**Figure 1E-G**). According to relative fluorescence intensity the fluorescence signal
213 recovered rapidly within FIT NBs (**Figure 1F**), and the calculated mobile fraction of the
214 NB protein was on average 80% (**Figure 1G**). Shape analysis of FIT NBs showed that the
215 NBs reached a high circularity score (**Figure 1H**). According to Wang et al. (2021),
216 fluorescence recovery and circularity scores as the ones measured for FIT NBs reflect
217 high mobility and circular shape. Thus, FIT NBs behave in a liquid-like manner suggesting
218 that LLPS might be the mechanism leading to FIT NB formation.
219 In summary, FIT-GFP forms light-inducible FIT NBs in roots and upon transient
220 expression in *N. bethamiana* leaf epidermis cells. The developed standardized FIT NB
221 analysis procedure was well suited for investigating dynamic properties of light-induced
222 FIT NBs and characterizing them as the likely result of LLPS. Because of these properties,
223 it is justified to term them 'FIT NBs'. We hypothesized that NB formation is a feature of the
224 FIT protein that provides regulatory specificity, and we subsequently investigated this
225 hypothesis using the developed standardized FIT NB analysis procedure in all subsequent
226 assays below.

227 **FIT forms homodimeric complexes preferentially in NBs, dependent on Ser271/272**

228 Next, we asked which properties of the FIT protein enable NB formation. Residue
229 Ser271/272 is important for the homo- and heterodimerization capacity of FIT (Gratz et
230 al., 2019). We therefore asked whether this site has an influence on FIT NB formation,
231 and we compared the ability for NB formation of phospho-mutated FIT with that of wild-
232 type FIT-GFP protein. In the work of Gratz et al. (2019), the phospho-mimicking
233 FITmS272E protein did not show significant changes in its behavior compared to wild-

234 type FIT. However, the FITmSS271AA-GFP mutant was less able to mediate induction of
235 iron deficiency responses and its properties differed from wild-type FIT-GFP (Gratz et al.,
236 2019). Hence, we focused on comparing the nuclear NB-forming characteristics between
237 wild-type FIT-GFP and FITmSS271AA-GFP mutant.

238 FITmSS271AA-GFP also localized to NBs. The formation of FITmSS271AA NBs
239 was delayed in time (**Figure 2A**; t=15 instead of t=5). While FIT-GFP NB formation started
240 in the first minutes after excitation and was fully present after 5 min (**Supplemental**
241 **Movie S1A**), FITmSS271AA-GFP NB formation occurred earliest 10 min after excitation
242 and was fully visible after 15 min (**Supplemental Movie S1C**). In addition, NB number
243 and size of FITmSS271AA-GFP were decreased in comparison to the ones from wild-type
244 FIT-GFP (**Figure 2, B and C**). Hence, the dynamics of NB formation were dependent on
245 Ser271/272.

246 The process of condensation is facilitated when proteins possess IDRs, since,
247 importantly, IDRs may engage in numerous interactions in space due to rapid
248 conformational changes (Tarczewska and Greb-Markiewicz, 2019; Emenecker et al.,
249 2020). The three-dimensional conformation of wild-type FIT had predicted stretches of
250 intrinsic disorganization, peaking before and at the basic region of the bHLH domain, and
251 two in the C-terminal part, one of them around the Ser271/272 site (termed $IDR^{Ser271/272}$;
252 **Supplemental Figure S2A**). In contrast, in the FITmSS271AA mutant this C-terminal
253 region was no longer classified as IDR (**Supplemental Figure S2B**). This underlined the
254 significance of the Ser271/272 site, not only for interaction (Gratz et al., 2019) but also for
255 FIT NB formation (**Figure 2**).

256 We then tested whether FIT homodimerization was preferentially associated with
257 NB formation. For that, we investigated whether FIT-GFP shows a differentiated
258 homodimerization strength, first, inside the NBs versus the nucleoplasm (NP), and
259 second, as wild-type FIT versus the mutant FITmSS271AA-GFP protein by performing
260 anisotropy (or homo-FRET) measurements. Energy transfer between the same kind of
261 fluorescently tagged proteins leads to depolarization of the emitted light (Stahl et al., 2013;
262 Weidtkamp-Peters et al., 2022). Fluorescence anisotropy (FA) describes this
263 depolarization and gives hints on the dimerization and oligomerization status of a protein
264 as the FA value decreases (**Figure 3A**). We measured FA before (t=0) and after NB
265 formation (t=5 for FIT and t=15 for FITmSS271AA), and analyzed the homodimerization
266 strength for the whole nucleus, the NBs, and the residual NP (**Figure 3B-D**). Free GFP

267 and GFP-GFP constructs were used as references for monomers and dimers (**Figure 3C**
268 **and D**).
269 Whole nucleus FA values were lower at t=5 than at t=0 for FIT-GFP. Additionally,
270 FA values were lower within the NBs compared to the NP (**Figure 3C**). Compared to wild-
271 type FIT-GFP, FA values were not reduced for mutant FITmSS271AA-GFP at t=15
272 compared to t=0. Also, the FA values did not differ between NBs and NP for the mutant
273 protein and did not show a clear separation in homodimerizing/non-dimerizing regions
274 (**Figure 3D**) as seen for FIT-GFP (**Figure 3C**). Both NB and NP regions showed that
275 homodimers occurred very variably in FITmSS271AA-GFP.
276 In summary, wild-type FIT could be partitioned properly between NBs and NP
277 compared to FITmSS271AA mutant and rather form homodimers, presumably due its
278 $IDR^{Ser271/272}$ at the C-terminus. NBs were nuclear sites in which FIT formed preferentially
279 homodimeric protein complexes.

280 **FIT-bHLH039 interaction complexes preferentially accumulate in FIT NBs**

281 FIT engages in protein-protein interactions with bHLH039 to steer iron uptake
282 target gene induction in the nucleus, while mutant FITmSS271AA protein is less active in
283 interacting with bHLH039 (Gratz et al., 2019). Hence, we tested whether FIT also interacts
284 with bHLH039 preferentially inside NBs and whether mutant FITmSS271AA differs in this
285 ability from wild-type FIT protein. bHLH039 alone does not localize inside the nucleus but
286 requires FIT for nuclear localization (Trofimov et al., 2019), so that bHLH039 was not used
287 alone to test its subnuclear localization.
288 Upon co-expression, FIT-GFP and bHLH039-mCherry colocalized fully in NBs that
289 resembled the previously described FIT NBs. In the beginning, both proteins were
290 uniformly distributed within the nucleus (t=0), and later became localized in NBs (t=5;
291 **Figure 4A**).
292 We then examined the heterodimerization strength of FIT-GFP and bHLH039-
293 mCherry, and FITmSS271AA-GFP and bHLH039-mCherry by FRET-fluorescence
294 lifetime imaging microscopy (FRET-FLIM) measurements. In case of protein interaction
295 (close proximity, ≤10 nm), energy transfer between a fluorescently tagged donor and a
296 fluorescently tagged acceptor decreases the fluorescence lifetime of the donor
297 (**Figure 4B;** Borst and Visser, 2010; Weidtkamp-Peters and Stahl, 2017). We quantified
298 the fluorescence lifetime of FIT-GFP and FITmSS271AA-GFP respective of

299 heterodimerization before (t=0) and after NB formation (t=5 for FIT and t=15 for
300 FITmSS271AA) in the whole nucleus, in NBs, and in the NP (**Figure 4C-E**). FIT-GFP and
301 FITmSS271AA-GFP (donor only) served as negative controls.
302 Fluorescence lifetime was decreased for the pair FIT-GFP and bHLH039-mCherry
303 at t=5 within NBs compared to all other measured areas (**Figure 4D**). In contrast to that,
304 the fluorescence lifetime decreased for the pair FITmSS271AA-GFP and bHLH039-
305 mCherry at t=15 was not different between NBs and NP (**Figure 4E**). This indicated that
306 heterodimeric complexes accumulated preferentially in FIT NBs.
307 In summary, heterodimerization of FIT with bHLH039 was spatially concentrated in
308 NBs versus the remaining nuclear space and was less prominent for FITmSS271AA.
309 Hence, the capacity of FIT to form an active TF complex was coupled with its presence in
310 NBs. The occurrence of FIT homo- and heterodimerization preferentially in NBs suggests
311 that FIT protein interaction may drive condensation. We therefore concluded that FIT NBs
312 may be sites with active TF complexes for iron deficiency response regulation.

313 **FIT NBs colocalize with speckle components**

314 Numerous NB types are known, and they are associated with particular proteins
315 that are indicative of the NB type. To further understand the identity, dynamics, and
316 function of FIT NBs, we co-expressed FIT-GFP with seven different NB markers from The
317 Plant Nuclear Marker collection (NASC) and observed NB formation and protein
318 colocalization before (t=0) and after FIT NB formation (t=5). In cases where we detected
319 a colocalization with FIT-GFP, we analyzed the localization of NB markers also in the
320 single expression at t=0 and at t=5 after the 488 nm excitation, to detect potentially
321 different patterns in single and co-expression.
322 All seven NB markers were expressed together with FIT-GFP, and according to the
323 resulting extent of colocalization we subdivided them into three different types. The first
324 type (type I) did not colocalize with FIT-GFP neither at t=0 nor at t=5 (**Supplemental**
325 **Figure S3**). This was the case for the Cajal body markers coilin-mRFP and U2 snRNP-
326 specific protein U2B”-mRFP (**Supplemental Figure S3**; Lorković et al., 2004; Collier et
327 al., 2006). Coilin-mRFP localized into a NB within and around the nucleolus
328 (**Supplemental Figure S3A**). The NBs of U2B”-mRFP were also close to the nucleolus
329 (**Supplemental Figure S3B**). Hence, FIT-GFP was not associated with Cajal bodies.

330 The second type (type II) of NB markers were partially colocalized with FIT-GFP.
331 This included the speckle components ARGININE/SERINE-RICH45-mRFP (SR45) and
332 the serine/arginine-rich matrix protein SRm102-mRFP (**Figure 5**). SR45 is involved in
333 splicing and alternative splicing and is part of the spliceosome in speckles (Ali et al., 2003),
334 and was recently found to be involved in splicing of iron homeostasis genes (Fanara et
335 al., 2022). SRm102 is a speckle component (Kim et al., 2016). SR45-mRFP localized
336 barely in the NP but inside few and very large NBs that remained constant at t=0 and t=5.
337 FIT-GFP did not colocalize in those NBs at t=0, however, it colocalized with the large
338 SR45-mRFP NBs at t=5 (**Figure 5A**). FIT-GFP also localized in typical FIT NBs in the
339 residual NP at t=5 (**Figure 5A**). SRm102-mRFP showed low expression in the NP and
340 stronger expression in a few NBs that also remained constant at t=0 and t=5. FIT-GFP
341 colocalized with SRm102-mRFP in only few instances at t=5, but not t=0, while most FIT
342 NBs did not colocalize with SRm102-mRFP NBs (**Figure 5B**). Both SR45-mRFP and
343 SRm102-mRFP had the same localization pattern at t=0 and t=5, irrespective of FIT-GFP
344 co-expression or 488 nm excitation (**Supplemental Figure S4**). These type II NB markers
345 seemed to recruit FIT-GFP into NBs after 488 nm excitation that were present (pre-
346 existing) before FIT-GFP NB formation, while FIT-GFP localized additionally in separate
347 FIT NBs. Hence, FIT became associated with splicing components and speckles upon the
348 light trigger.
349 A third type (type III) of three NBs markers, namely UAP56H2-mRFP, P15H1-
350 mRFP, and PININ-mRFP, were fully colocalized with FIT-GFP (**Figure 6**). Until now, these
351 NB marker proteins are not well described in plants. UAP56H2 is a RNA helicase, which
352 is involved in mRNA export (Kammel et al., 2013). P15H1 was found as a putative
353 Arabidopsis orthologue of an exon junction complex component in humans (Pendle et al.,
354 2005), while PININ has a redundant role to its paralogue apoptotic chromatin
355 condensation inducer in the nucleus (ACINUS) in alternative splicing (Bi et al., 2021).
356 UAP56H2-mRFP and P15H1-mRFP did not localize in NBs and were not responsive to
357 the 488 nm excitation when expressed alone or together with FIT-GFP at t=0 (**Figure 6,**
358 **A and B and Supplemental Figure S4, C and D**). When co-expressed with FIT-GFP and
359 following the 488 nm excitation, at t=5, the two NB markers adopted the FIT NB pattern
360 and colocalized with FIT-GFP in FIT NBs (**Figure 6, A and B**). PININ-mRFP was also
361 uniformly distributed in the nucleus at t=0 like FIT-GFP and fully colocalized with FIT NBs
362 at t=5 (**Figure 6C**). But curiously, PININ-mRFP showed a very different localization in the

363 single expression. Predominately, it localized to a very large NB besides several small
364 NBs with no expression in the NP at t=0 and at t=5 (**Supplemental Figure S4E**). Thus,
365 FIT-GFP recruited these type III NB marker and speckle proteins fully into FIT NBs. Since
366 type III NB markers are also potentially involved in splicing and mRNA export from the
367 nucleus, these same functions may be relevant in FIT NBs.

368 Taken together, the colocalization studies underlined the dynamic behavior of
369 inducible FIT NB formation. FIT NBs had a speckle function, in which on the one hand FIT
370 was recruited itself into pre-existing splicing-related NBs (SR45-mRFP and SRm102-
371 mRFP, type II), while on the other hand it also recruited speckle-localized proteins into
372 FIT NBs (UAP56H2-mRFP, P15H1-mRFP, and PININ-mRFP, type III).

373 **PB components influence FIT NB localization and formation**

374 PBs are plant-specific condensates which harbor various light signaling
375 components (Kircher et al., 2002; Bauer et al., 2004). Among them are the bHLH TFs of
376 the PIF family. As key regulators of photomorphogenesis, they integrate light signals in
377 various developmental and physiological response pathways (Leivar and Monte, 2014;
378 Pham et al., 2018). Indeed, PIF4 may control iron responses in Arabidopsis based on
379 computational analysis of iron deficiency response gene expression networks
380 (Brumbarova and Ivanov, 2019) and both PIF proteins intersect with blue light signaling
381 (Ni et al., 1998; Oh et al., 2004; Pedmale et al., 2016). We tested in the same manner as
382 described above for NB markers, whether FIT NBs coincide with two of the described PB
383 markers, PIF3-mCherry and PIF4-mCherry (Van Buskirk et al., 2014; Qiu et al., 2019,
384 2021).

385 We detected distinct localization patterns for PIF3-mCherry and PIF4-mCherry
386 (**Figure 7**). At t=0, PIF3-mCherry was predominantly localized in a single large PB
387 (**Figure 7A**). Localization of single expressed PIF3-mCherry remained unchanged at t=0
388 and t=15 (**Supplemental Figure S5A**). Upon co-expression, FIT-GFP was initially not
389 present in PIF3-mCherry PB at t=0. After 488 nm excitation, FIT-GFP accumulated and
390 finally colocalized with the large PIF3-mCherry PB at t=15, while the typical FIT NBs did
391 not appear (**Figure 7A**).

392 PIF4-mCherry localized in two different patterns, and both differed substantially
393 from that of PIF3-mCherry. In the one pattern at t=0, PIF4-mCherry was not localized to
394 any PBs, but instead was uniformly distributed in the NP as was the case for FIT-GFP.

395 Such a pattern was also seen at t=15, and then neither PIF4-mCherry nor FIT-GFP were
396 localized in any PBs/NBs (**Figure 7B**). In the other pattern, PIF4-mCherry and FIT-GFP
397 localized in multiple PBs at t=0 and t=15, whereas none of them corresponded
398 morphologically to the typical FIT NBs (**Figure 7C**). The same two localization patterns
399 were also found for PIF4-mCherry in the single expression, whereby 488 nm excitation
400 did not alter PIF4-mCherry localization (**Supplemental Figure S5, B and C**).
401 Hence, FIT was able to localize to PBs when co-expressed with PIF3 and PIF4,
402 raising the possibility that FIT is a key regulator to cross-connect iron acquisition regulation
403 and light signaling pathways. Again, colocalization demonstrates the dynamic behavior of
404 FIT-GFP.

405 **Blue light has a promoting effect on iron acquisition responses downstream of FIT**

406 Previous studies have shown that iron uptake by FIT is diurnally and circadian
407 clock-regulated (Vert et al., 2003; Santi and Schmidt, 2009; Salomé et al., 2013). Knowing
408 that FIT NB formation was light-dependent as well as promoting the interaction of the FIT-
409 bHLH039 complex, and that FIT NBs were colocalizing with light signaling and PB
410 components, we reasoned that plants exposed to the FIT NB-forming light cues may show
411 differential FIT-dependent iron uptake responses with respect to control plants exposed
412 to the regular light conditions. To test this, we grew wild-type Arabidopsis plants for 5 d
413 under iron sufficient and iron deficient conditions under white light and exposed the plants
414 additionally for 1 d to blue light. As a control for light quality, we also included exposure to
415 red and far-red light and darkness besides the regular white light. We measured molecular
416 iron uptake responses known to be under the control of FIT-bHLH039 in roots (Gratz et
417 al., 2019).
418 Iron reductase activity is increased in roots when FIT and bHLH039 are activated
419 in response to iron deficiency in our growth system (Gratz et al., 2019). Iron reductase
420 activity was higher under iron deficient conditions compared to iron sufficient conditions
421 under all white light controls, as expected (**Figure 8A-D**). Interestingly, when seedlings
422 were exposed to blue light for a day, they induced iron reductase activity in the iron
423 deficient versus iron sufficient condition more than in the white light control (**Figure 8A**).
424 On the other hand, exposure to red light did not change the iron reductase activity
425 compared to the white light control (**Figure 8B**), while exposure to far-red light or darkness
426 abolished the induction (**Figure 8, C and D**). Hence, only exposure to blue light had an

427 extra promoting effect on iron uptake in the seedlings compared with the other tested light
428 qualities.

429 Increased iron acquisition under iron deficiency and enhanced iron reductase
430 activity require FERRIC REDUCTASE-OXIDASE2 (FRO2) protein (Yi and Guerinot, 1996;
431 Robinson et al., 1999), and *FRO2* to be induced, along with *IRON REGULATED*
432 *TRANSPORTER1* (*IRT1*; Eide et al., 1996; Korshunova et al., 1999). *FRO2* and *IRT1* are
433 target genes of FIT-bHLH039 in our growth system (Gratz et al., 2019, 2020). As a readout
434 of the activity of the FIT-bHLH039 complex, we examined gene regulation of *FRO2* and
435 *IRT1* as well as *FIT* and *BHLH039* under the same light conditions as described above.
436 Previously, it was shown that the expression of *IRT1* and *FRO2* was downregulated under
437 iron deficient conditions in darkness compared to iron deficient conditions in white light,
438 while the opposite was true for *FIT* (Santi and Schmidt, 2009).

439 Under white light conditions, gene expression for all four genes was tested in four
440 independent samples. In 15 out of the 16 cases, gene expression of *FIT*, *BHLH039*, *FRO2*
441 and *IRT1* was significantly higher under iron deficient than sufficient conditions, as
442 expected, and in only one case for *FIT*, it was similar and not significantly enhanced
443 (**Figure 9A-P, with exception of E**, *FIT*). Under blue light, *FIT* and *BHLH039* expression
444 was induced upon iron deficiency in the same manner as in white light (**Figure 9, A and**
445 **B**), whereas *FRO2* and *IRT1* were induced to a higher level in response to iron deficiency
446 in blue light versus white light (**Figure 9A-D**). Again, plant responses were different upon
447 exposure to other light conditions. *FIT* and *IRT1* were similarly induced, while *BHLH039*
448 and *FRO2* were even less induced by iron deficiency under red light than white light
449 (**Figure 9E-H**). In both, the far-red light and darkness situations, *FIT* was induced under
450 iron deficiency versus sufficiency, while on the other side, *BHLH039*, *FRO2* and *IRT1*
451 were not induced at all in these light conditions (**Figure 9I-P**). *FIT* was similarly induced
452 under far-red light and white light (**Figure 9I**), whereas in darkness it was even induced
453 to higher level (**Figure 9M**), as previously reported (Santi and Schmidt, 2009).

454 Since colocalization with NB markers showed partial or full colocalization with FIT
455 within NBs (**Figure 5 and 6**), we included gene expression analysis on some of the
456 previously described intron retention (IR) splicing variants of *FIT*, *BHLH039*, and FIT
457 target genes *IRT1* and *FRO2* (Li et al., 2013, 2016a) to see whether differential alternative
458 splicing would be detectable under the same experimental conditions that led to FIT NB
459 formation in Arabidopsis (**Figure 1A**). For this, we grew wild-type Arabidopsis plants

460 under iron sufficient and iron deficient conditions for 5 d under white light and exposed the
461 plants for 1.5 or 2 h to blue light.
462 IR splicing variants occurred to higher extent under iron deficient conditions
463 compared to iron sufficient conditions regardless of the light condition (**Supplemental**
464 **Figure S6**). After normalization of gene expression of plants grown under iron deficient
465 conditions with plants grown under iron sufficient conditions, no difference between the
466 respective gene and its splicing variants could be shown (**Supplemental Figure S7**).
467 To sum up, the FIT-bHLH039-dependent target gene expression is similarly light
468 quality-dependent as the FIT-bHLH039-dependent iron reductase activity but not the
469 splicing variant abundance of the tested genes. Hence, very interestingly, blue light cues
470 which lead to FIT NB formation, promoted FIT-bHLH039-dependent iron uptake
471 responses, fitting with the above finding that FIT NBs are linked with active TF complexes
472 in condensates. However, a differential effect of NB-forming conditions and alternative
473 splicing was not found suggesting that FIT NBs do not primarily affect alternative splicing
474 processes of the tested iron deficiency marker genes.

475 **Discussion**

476 In this study, we uncovered a previously unknown phenomenon, the blue light-
477 induced and reversible accumulation of FIT condensates in FIT NBs. LLPS was most
478 likely the underlying mechanism for this highly dynamic process. FIT NBs were enriched
479 in active FIT TF complexes that are required for iron deficiency gene regulation. FIT
480 associated with speckles and PBs in a highly dynamic fashion, indicating a function in
481 transcriptional and posttranscriptional control. Blue light exposure resulted in enhanced
482 molecular FIT-bHLH039-dependent iron acquisition responses but not a different effect
483 on alternative splicing pathways of *FIT*, *BHLH039*, *IRT1* and *FRO2*. Based on these data,
484 we propose that FIT NBs are dynamic microenvironments with active FIT TF complexes
485 that possibly are hubs to enhance and cross-connect transcriptional iron deficiency gene
486 expression with posttranscriptional regulation and environmental signaling.

487 **A standardized procedure for FIT NB induction was crucial to delineate the**
488 **characteristics of FIT NBs in reliable manner**

489 We were able to characterize the nature and potential function of light-induced FIT
490 NBs using quantitative microscopy-based techniques and a standardized NB analysis
491 procedure. Roots also formed NBs, however their direct inspection was not possible using

492 the same microscopy techniques. Since condensation depleted FIT protein in the
493 nucleoplasm, the remaining low FIT protein concentration can be the reason why FIT NBs
494 remained few in number in the Arabidopsis root cells. The *N. benthamiana* protein
495 expression system did not present these limitations and high-quality measurement data
496 were obtained for all experimental series. Furthermore, this expression system is a well-
497 established and widely utilized system in plant biology (Martin et al., 2009; Bleckmann et
498 al., 2010; Leonelli et al., 2016; Burkart et al., 2022). The developed standardized assay
499 generated reliable and accurate data for statistical analysis and quantification to conclude
500 about FIT NB characteristics.

501 Condensation likely explains the reduced mobility of FIT-GFP versus
502 FITmSS271AA-GFP seen in a previous study (Gratz et al., 2019). In liquid state,
503 condensates are more mobile than in the solid one. The condensate formation was
504 reversible, speaking in favor of a liquid state of the condensates. According to FRAP data,
505 FIT NBs maintained a dynamic exchange of FIT protein with the surrounding NP. FIT NBs
506 were also mostly of circular shape. Circular condensates appear as droplets, in contrast
507 to solid-like condensates that are irregularly shaped (Shin et al., 2017). These
508 characteristics speak in favor of liquid-like features, suggesting that LLPS underlies FIT
509 NB formation. A similar situation was described for CRY2 PBs, which were also reversible
510 and of circular shape with mobile protein inside PBs (Wang et al., 2021). bHLH039 was
511 found accumulated in cytoplasmic foci at the cell periphery (Trofimov et al., 2019). In such
512 foci, bHLH039 was immobile, and we suspect it was in a non-functional state in the
513 absence of FIT. This underlines the understanding that liquid condensates such as FIT
514 NBs are dynamic microenvironments, whereas immobile condensates point rather
515 towards a solid and pathological state (Shin et al., 2017).

516 Additionally, the partial and full colocalization of FIT NBs with various previously
517 reported NB markers confirm that FIT indeed accumulates in and forms NBs. Since
518 several of NB body markers are also behaving in a dynamic manner, this corroborates the
519 formation of dynamic FIT NBs affected by environmental signals.

520 In conclusion, the properties of liquid condensation and colocalization with NB
521 markers, along with the findings that it occurred irrespective of the fluorescence protein
522 tag preferentially with wild-type FIT, allowed us to coin the term of ‘FIT NBs’.

523 **IDR$^{Ser271/272}$ was crucial for interaction and NB formation of FIT**

524 FIT NBs were hotspots for homodimeric and heterodimeric FIT interaction, allowing
525 to assume that they are integrated in the iron deficiency response as interaction hubs.
526 These abilities distinguished wild-type FIT and mutant FITmSS271AA, indicating that wild-
527 type FIT is a multivalent protein and that IDR$^{Ser271/272}$ is important for that. FIT protein may
528 interact via the helix-loop-helix interface and via its C-terminus containing the IDR (Lingam
529 et al., 2011; Le et al., 2016; Gratz et al., 2019) to be multivalent. The flexible IDRs adapt
530 to multiple protein partners and are therefore crucial for multivalency (Tarczewska and
531 Greb-Markiewicz, 2019; Emenecker et al., 2020; Salladini et al., 2020), and the amino
532 acid composition of IDRs is important for condensation (Powers et al., 2019; Emenecker
533 et al., 2021; Huang et al., 2022). Very interestingly, posttranslational modification in form
534 of phosphorylation within IDRs may regulate condensate formation (Owen and
535 Shewmaker, 2019). Ser271/272 is targeted by a FIT-interacting protein kinase that can
536 affect FIT activity and FIT phosphorylation (Gratz et al., 2019). Hence, phosphorylation of
537 Ser271/272 might perhaps be a trigger for NB formation *in vivo*. It could not be
538 distinguished in this study whether FIT homodimers were a prerequisite for the localization
539 of bHLH039 in NBs or whether FIT-bHLH039 complexes also initiated NBs on their own.

540 **Formation of FIT NB is highly dynamic**

541 FIT may have formed FIT NBs as entirely newly formed structures upon the light
542 trigger. But it is also possible that FIT joined pre-existing NBs, which then became the
543 structures we termed FIT NBs. Partial or full colocalization of FIT-GFP with NB and PB
544 markers revealed the remarkably high and intriguing dynamic nature of FIT NBs and
545 suggests that both possibilities are plausible. FIT NBs are light-triggered, and this speaks
546 in favor of pre-existing NBs. Since FIT does not possess light-responsive domains, it is
547 most likely that a light-responsive protein must be inducing FIT NB formation. The basic
548 leucine zipper TF ELONGATED HYPOCOTYL5 (HY5) could be a good candidate, since
549 HY5 is a mobile protein involved in iron acquisition in tomato (Gao et al., 2021; Guo et al.,
550 2021) and acts positively on iron uptake and gene expression of *FIT*, *FRO2*, and *IRT1* in
551 Arabidopsis (Mankotia et al., 2023). Possibly activation and condensation involve not only
552 the studied NB and PB markers but also potentially signaling proteins or further scaffold
553 proteins that are part of the multivalent protein complexes in FIT NBs. On the other hand,
554 FIT-GFP accumulated not only in FIT NBs but also in the pre-existing NBs with type II NB

555 markers (SR45 and SRm102) after the FIT NB induction. In this respect, type II markers
556 were similar to PIF3 and PIF4. FIT-GFP was recruited to pre-existing PBs and again only
557 after the light trigger. Interestingly, typical FIT NB formation did not occur in the presence
558 of PB markers, indicating that they must have had a strong effect on recruiting FIT. This
559 is interesting because the partially colocalizing SR45, PIF3 and PIF4 are also dynamic
560 NB components. Active transcription processes and environmental stimuli affect the sizes
561 and numbers of SR45 speckles and PB (Ali et al., 2003; Legris et al., 2016; Meyer, 2020).
562 This may indicate that, similarly, environmental signals might have affected the
563 colocalization with FIT and resulting NB structures in our experiments. Another factor of
564 interference might also be the level of expression. Overall, the dynamics of FIT
565 colocalization with type II NB and PB markers suggest that these condensates dictated
566 FIT condensation in their own pre-existing NBs/PBs. This recruiting process could be
567 navigated via protein-protein interaction since this is the driving force of condensation
568 (Kaiserli et al., 2015; Emenecker et al., 2020).

569 On the other side, the full colocalization of FIT with type III NB markers speaks in
570 favor of a *de novo* FIT NB formation. The three fully colocalizing type III NB markers
571 (UAP56H2, P15H1 and PININ) accumulated only in FIT NBs upon co-expression with FIT
572 and mostly not on their own. The same was true for bHLH039, that joined FIT in FIT NBs,
573 showing that FIT not only facilitated bHLH039 nuclear localization (Trofimov et al., 2019)
574 but also condensation. Interestingly, FIT was able to change PININ nuclear localization.
575 In single expression, PININ was localized to a major large NB, but in colocalization with
576 FIT it joined the typical FIT NBs. This suggests that FIT dictates bHLH039 and type III NB
577 markers and highlights that FIT is also able to set the tone for NB formation. Hence, FIT
578 can recruit other proteins into NBs, and it is possible that FIT forms its own NBs. Protein-
579 protein interaction could underly this recruitment, as evident for bHLH039 (Kaiserli et al.,
580 2015; Emenecker et al., 2020).

581 **FIT NBs have speckle characteristics**

582 Since the type II and III markers are splicing components, the colocalization studies
583 suggest that FIT NBs are speckles, in agreement with the dynamic nature of FIT NBs.
584 Speckles are highly dynamic, forming around transcriptionally active sites in the
585 interchromatin regions recruiting several protein functions like mRNA synthesis,
586 maturation, splicing and export (Reddy et al., 2012; Galganski et al., 2017). Co-

587 transcriptional splicing in plants is also recently rising (Nojima et al., 2015; Zhu et al., 2018;
588 Chaudhary et al., 2019). Mediator complex condensation was shown to drive
589 transcriptional control (Boija et al., 2018) and interestingly, FIT was also shown to interact
590 with Mediator complexes, directly and indirectly (Yang et al., 2014; Zhang et al., 2014).
591 Besides, other studies suggest TF condensation to be involved in transcriptional
592 regulation (Kaiserli et al., 2015; Boija et al., 2018; Brodsky et al., 2020; Huang et al., 2022).
593 The type II speckle component SR45, is a highly mobile protein in speckles and required
594 phosphorylation for proper speckle localization (Ali et al., 2003; Reddy et al., 2012). These
595 processes fit well to the described FIT NB attributes. The characterization of FIT NBs as
596 speckles is interesting because regulation of splicing and epigenetic regulation is
597 associated with both, iron deficiency gene expression and SR45 (Fanara et al., 2022;
598 Mikulski et al., 2022). UAP56H2, P15H1, and PININ (type III) are connected to SR45 and
599 SRm102 (type II) in mammalian cells as all being part of the exon junction complex and
600 interacting with each other (Lin et al., 2004; Pendle et al., 2005). This is an interesting
601 parallel, as it suggests that type II and type III marker localization is conserved across
602 kingdoms, underlying the ancient nature of condensates. Indeed, SR45 and PININ located
603 both to a very large NB in non-induced cells. This opens the possibility that the two
604 proteins might localize to the same type of speckle, as also might FIT. Taken together,
605 the observations confirm the high diversification and complexity of FIT NBs and speckles
606 (Lorković et al., 2008) and it is tempting to speculate that FIT might regulate splicing and
607 alternative splicing of its target genes by recruiting speckle components.
608 However, further studies are needed to investigate whether the blue light treatment
609 resulting in FIT NBs causes alternative splicing compared with white light. The previously
610 reported intron retention events (Li et al., 2013) were confirmed in our study but a
611 differential effect of light was not apparent, although it may be rare and might have been
612 masked by non-reactive nuclear events.

613 **Model and physiological integration of FIT NBs**

614 FIT NBs may serve the rapid rearrangement of TFs to enhance target gene
615 expression and subsequent physiological responses during a high photosynthetic period.
616 The formation and dissociation of NBs could be a fast way to adjust iron uptake and
617 specifically uncouple *IRT1* and *FRO2* from FIT regulation and therefore adapt even better
618 to environmental changes, possibly triggered by phosphorylation (Gratz et al., 2020). The

619 rapid speed by which FIT NB appeared within 5 min in *N. benthamiana* leaf cells speaks
620 in favor of protein rearrangement rather than protein synthesis. The long duration of FIT
621 NB formation after blue light induction in Arabidopsis roots suggests that signal
622 transduction was more complex and possibly involved intracellular or even cell-to-cell and
623 long-distance leaf-to-root signaling. A long-distance signal or a signaling cascade
624 triggered by light might be involved in FIT NB formation. CRY1/CRY2 and HY5 are
625 promising candidates for further studies (Gao et al., 2021; Guo et al., 2021; Mankotia et
626 al., 2023). In order to undergo phase separation, a certain protein concentration must be
627 reached (Bracha et al., 2018). Since FIT protein is subject of proteasomal turnover in
628 roots, FIT NB formation may depend on FIT protein interaction partners in roots that need
629 to be activated (Lingam et al., 2011; Meiser et al., 2011).
630 In summary, FIT localizes to dynamic and reversible NBs. FIT NBs contain active
631 TF complexes for iron acquisition gene expression and are speckles that link
632 transcriptional with posttranscriptional regulation. The appearance of FIT NBs is inducible
633 by blue light, a condition that promotes iron mobilization responses, and light regulated
634 PB components are connected with FIT NBs and vice versa (**Figure 10**). It will be
635 interesting in the future to test hormonal and environmental triggers that may stabilize FIT
636 protein prior to examining the initiation of FIT NBs in root physiological situations. Further
637 studies are needed to determine whether FIT NBs might have a transcriptional and
638 posttranscriptional function to regulate unknown FIT target sites.

639 **Materials and methods**

640 **Plant material and growth conditions**

641 *Arabidopsis thaliana* experiments were conducted with the Col-0 accession.
642 Arabidopsis line FIT_{pro}:FIT-GFP used for imaging was obtained as follows: First, the
643 FIT_{pro}:FIT-GFP construct was obtained in a plant gene expression binary vector via
644 GreenGate cloning (Lampropoulos et al., 2013). *FIT* promoter sequence of 2012 bp
645 upstream of the CDS was cloned into pGGA000 entry vector using pFIT GG fw and pFIT
646 GG rv primers with respective overhang sequences (**Supplemental Table S1**). FIT CDS
647 (954 bp, without stop codon) was cloned into pGGC000 entry vector using cFIT GG fw
648 and cFIT GG rv primers with respective overhang sequences (**Supplemental Table S1**).
649 The final construct was created via the GreenGate reaction with the pGGZ001 destination
650 vector, containing the entry vectors pGGA000 FIT promoter, pGGB003 *B-dummy* for N-
651 tag, pGGA000 FIT CDS, pGGD001 *linker*-GFP, pGGE009 *UBQ10* terminator, and
652 pGGF001 $p^{d}MAS^{e}$:$BastaR^{f}$:$t^{g}MAS$, and verified by sequencing. The plasmid was
653 transferred to *Rhizobium radiobacter* pSOUP strain (GV3103). Transgenic plants (in Col-
654 0 wild-type background) were obtained by floral dip transformation (Clough and Bent,
655 1998) and subsequent Basta selection. *Arabidopsis thaliana* 2x35S_{pro}:FIT-GFP/*fit-3* line
656 used for imaging was previously described in Gratz et al. (2019).

657 *Arabidopsis thaliana* FIT_{pro}:FIT-GFP and 2x35S_{pro}:FIT-GFP/*fit-3* seedlings were
658 used for localization studies. Seeds were sterilized and grown upright on Hoagland
659 medium plates (macronutrients: 1.5 mM $Ca(NO_3)_2 \cdot 4H_2O$, 0.5 mM KH_2PO_4, 1.25 mM
660 KNO_3, 0.75 mM $MgSO_4 \cdot 7H_2O$; micronutrients: 0.075 µM $(NH_4)6Mo_7O_{24} \cdot 4H_2O$, 1.5 µM
661 $CuSO_4 \cdot 5H_2O$, 50 µM H_3BO_3, 50 µM KCl, 10 µM $MnSO_4 \cdot H_2O$, 2 µM $ZnSO_4 \cdot 7H_2O$;
662 1.4 % (w/v) plant agar, 1 % (w/v) sucrose, pH 5.8) with no iron supply for 5 d under long
663 day conditions (16 h light/8 h dark) at 21°C in a plant chamber (CLF Plant Climatics) under
664 white light (120 µmol m^{-2} s^{-1}).

665 For iron reductase activity assays and gene expression analysis, *Arabidopsis*
666 *thaliana* seedlings were sterilized and grown upright on Hoagland medium plates with
667 either no iron supply or with 50 µM FeNaEDTA supply for 5 d under long day conditions
668 (16 h light/8 h dark) at 21°C in a plant chamber (CLF Plant Climatics) under white light
669 (120 µmol m^{-2} s^{-1}). For different light treatments plates were transferred to LED light
670 chambers (CLF Plant Climatics) for 1.5 h-2 h (splicing variant gene expression analysis)
671 or 1 d under continuous blue light (70 µmol m^{-2} s^{-1}), continuous red light (55 µmol m^{-2} s^{-1}),

672 continuous far-red light (65 µmol m^{-2} s^{-1}) or darkness. White light was used as control
673 (125 µmol m^{-2} s^{-1}).
674 *Nicotiana benthamiana* plants were grown in the greenhouse facility for approx. 4
675 weeks under long day conditions (16 h light/8 h dark) for use in transient protein
676 expression experiments.

677 **Root iron reductase activity assay**

678 6-d-old seedlings were grown as described in the text. Root iron reductase activity
679 was determined as described in Le *et al.* (2016). Plants were washed with 0.1 M
680 $Ca(NO_3)_2 \cdot 4H_2O$ and subsequently incubated for 1 h in darkness at room temperature in
681 the iron reductase solution (300 µM Ferrozine, 100 µM FeNaEDTA). The absorbance of
682 the ferrozine-Fe^{2+} complex was measured at 562 nm and used to calculate the root iron
683 reductase activity normalized to root fresh weight.

684 **Gene expression analysis by RT-qPCR**

685 5-d or 6-d-old seedlings were grown as described in the text. The reverse
686 transcription-real time-quantitative polymerase chain reaction (RT-qPCR) procedure and
687 analysis is described in Abdallah and Bauer (2016). Briefly, plant material was harvested,
688 using three biological replicates, and shock frozen. RNA was extracted (peqGOLD Plant
689 RNA Kit, PEQLAB). Subsequently, an amount of 0.5 µg of total RNA was used for cDNA
690 synthesis (Thermo Scientific). Diluted cDNA, SYBR green master mix (Thermo Scientific)
691 and respective primers (**Supplemental Table S1**) were pipetted in a 96 well plate and
692 qPCR was performed with two technical duplicates with the CFX96 Touch™ Real-Time
693 PCR Detection System (Bio-Rad). qPCR data were analyzed, and quantification was
694 obtained according to the mass standard curve analysis procedure. Normalization was
695 performed using the reference gene *ELONGATION FACTOR1A* (*EFc*). Statistical analysis
696 was performed with absolute normalized gene expression levels.

697 **Microscopy of *Arabidopsis thaliana* seedlings**

698 Protein localization studies in roots of 5-d-old seedlings of the *Arabidopsis thaliana*
699 line FIT_{pro}:FIT-GFP and 2x35S_{pro}:FIT-GFP/*fit-3* were performed with the widefield
700 microscope ELYRA PS (Zeiss) equipped with a EMCCD camera. To induce FIT NB
701 formation, whole seedlings were exposed to 488 nm laser light for several minutes. GFP
702 was excited with a 488 nm laser and detected with a BP 495-575 + LP 750 beam splitter.

703 Images were acquired with the C-Apochromat 63x/1.2 W Korr M27 (Zeiss) objective, pixel
704 dwell time of 1.6 µs and frame size of 512x512. Pictures were processed with the
705 manufacturer's software ZEN lite (Zeiss).

706 **Generation of fluorescent constructs**

707 All constructs used in this study are listed in **Supplemental Table S2**. Generation
708 of fluorescent translational C-terminal fusion of PIF3 and PIF4 with mCherry was
709 performed with Gateway Cloning. CDS of *PIF3* was amplified with the PIF3 GW fw and
710 PIF3 GW rv primers (**Supplemental Table S1**), and CDS of *PIF4* was amplified with the
711 PIF4 GW fw and PIF4 GW rv primers (**Supplemental Table S1**), and introduced into the
712 entry vector pDONR207 via the BP reaction (Life Technologies) and subsequently into
713 the inducible pABind $35S_{pro}$:mCherry destination vector (Bleckmann et al., 2010) via the
714 LR reaction (Life Technologies). Finally, *Rhizobium radiobacter* was transformed with the
715 constructs for transient transformation of *Nicotiana benthamiana* leaf epidermal cells.

716 **Transient transformation of *Nicotiana benthamiana* leaf epidermal cells**

717 Transient protein expression was performed in *Nicotiana benthamiana* leaf
718 epidermal cells according to Bleckmann et al. (2010). This was performed for localization
719 studies, FRAP measurements, anisotropy (homo-FRET) measurements, FRET-FLIM
720 measurements, and NB quantification. Cultures of *Rhizobium radiobacter* containing the
721 construct of interest (**Supplemental Table S2**) were incubated overnight and cell were
722 pelleted and dissolved in AS medium (250 µM acetosyringone (in DMSO), 5 % (w/v)
723 sucrose, 0.01 % (v/v) silwet, 0.01 % (w/v) glucose). An OD_{600nm} of 0.4 was set for all
724 constructs. A *Rhizobium radiobacter* strain containing the silencing repressor p19 vector
725 (Shamloul et al., 2014) was used additionally for bHLH039-mCherry to enhance
726 expression. After 1 h incubation on ice the suspension was infiltrated with a syringe into
727 the abaxial side of the leaf. *Nicotiana benthamiana* plants were kept under long day
728 conditions (16 h light/8 h dark) in the laboratory after infiltration. Imaging was performed
729 2-3 d after infiltration. Expression of constructs with an inducible 35S promoter was
730 induced 16 h prior to imaging with β-estradiol (20 µM β-estradiol (in DMSO), 0.1 % (v/v)
731 Tween 20). In total, 3-4 differently aged leaves of 2 plants were infiltrated and used for
732 imaging. One infiltrated leaf with homogenous presence of one or two fluorescence
733 proteins was selected, depending on the aim of the experiment, and ca. 30 cells were
734 observed. Images are taken from 3-4 cells, one representative image is shown.

735 **Confocal microscopy**

736 For localization studies a confocal laser scanning microscope LSM780 (Zeiss) was
737 used. Imaging was controlled by the ZEN 2.3 SP1 FP3 (Black) (Zeiss) software. GFP was
738 excited with a 488 nm laser and detected in the range of 491-553 nm. mCherry and mRFP
739 were excited with a 561 nm laser and detected in the range of 562-626 nm. Fluorophore
740 crosstalk was minimized by splitting of the excitation tracks and reduction of emission
741 spectrum overlap. Images were acquired with the C-Apochromat 40x/1.20 W Korr M27
742 (Zeiss) objective, zoom factor of 8, pinhole set to 1,00 AU, pixel dwell time of 1.27 µs and
743 frame size of 1.024x1.024. Z-stacks for quantification were taken with the same settings,
744 except with pixel dwell time of 0.79 µs and frame size of 512x512. Pictures were
745 processed with the manufacturer's software ZEN lite (Zeiss).

746 **Standardized FIT NB analysis procedure**

747 Following *Nicotiana benthamiana* leaf infiltration with *Rhizobium radiobacter*, FIT-
748 GFP protein expression was induced after 2-3 d by β-estradiol, as described above. 16 h
749 later, a leaf disc was excised and FIT-GFP fluorescence signals were recorded (t=0). The
750 leaf disc was excited with 488 nm laser light for 1 min. 5 min later, FIT-GFP accumulation
751 in FIT NBs was observed (t= 5 min). See **Supplemental Figure S1C**. This procedure was
752 modified by using different time points for NB analysis and different constructs
753 (**Supplemental Table S2**) and co-expression as indicated in the text. Imaging was
754 performed at the respective wavelengths for detection of GFP and mRFP/mCherry.

755 **FRAP measurements**

756 FRAP measurements (Bancaud et al., 2010; Trofimov et al., 2019) were performed
757 at the confocal laser scanning microscope LSM780 (Zeiss). Imaging was controlled by the
758 ZEN 2.3 SP1 FP3 (Black) (Zeiss) software. GFP was excited with a 488 nm laser and
759 detected in the range of 491-553 nm. Images were acquired with the C-Apochromat
760 40x/1.20 W Korr M27 (Zeiss) objective, zoom factor of 8, pinhole set to 2,43 AU, pixel
761 dwell time of 1.0 µs, frame size of 256x256, and 300 frames. After 20 frames, a NB was
762 bleached with 50 iterations and 100% 488 nm laser power. Fluorescence intensity was
763 recorded for the bleached NB (ROI), a non-bleached region equal in size to the NB (BG)
764 as well as for the total image (Tot). Values were calculated and processed in Excel
765 (Microsoft Corporation). Background subtraction and normalization to calculate the
766 relative fluorescence intensity was performed as follows: [(ROI(t)-BG(t)/Tot(T)-

767 BG(t))*(Tot(t0)-BG(t0)/ROI(t0)-BG(t0))]. The mobile fraction was calculated as follows:
768 [(F_{end}-F_{post})/(F_{pre}-F_{post})*100]. F_{pre} marks the average of the 20 values before bleaching,
769 F_{post} marks the value right after the bleaching, and F_{end} marks the average of the 280
770 values after the bleaching. Pictures were processed with the manufacturer's software ZEN
771 lite (Zeiss).

772 **Anisotropy (homo-FRET) measurements**

773 Anisotropy measurements (Stahl et al., 2013; Weidtkamp-Peters et al., 2022) were
774 performed at the confocal laser scanning microscope LSM780 (Zeiss) equipped with a
775 polarization beam splitter, bandpass filter (520/35), and a single-photon counting device
776 HydraHarp (PicoQuant) with avalanche photo diodes (τ-SPADs). Emission was detected
777 in parallel and perpendicular orientation. Rhodamine 110 was used to determine the G
778 factor to correct for the differential parallel and perpendicular detector sensitivity.
779 Calibration of the system was performed for every experiment and measurements were
780 conducted in darkness. Free GFP and GFP-GFP were used as references for mono- and
781 dimerization, respectively. GFP was excited with a linearly polarized pulsed (32 MHz)
782 485 nm laser and 0.05-1 µW output power. Measurements were recorded with a C-
783 Apochromat 40x/1.20 W Korr M27 (Zeiss) objective, zoom factor of 8, pixel dwell time of
784 12.5 µs, objective frame size of 256x256, and 40 frames. Measurements were controlled
785 with the manufacturer's ZEN 2.3 SP1 FP3 (Black) (Zeiss) software and SymPhoTime 64
786 (PicoQuant) software. SymPhoTime 64 (PicoQuant) software was used for analysis in the
787 respective regions of interest (whole nucleus, NB, NP) and to generate color-coded FA
788 value images. Minimal photon count was set to 200.

789 **FRET-FLIM measurements**

790 FRET-FLIM measurements (Borst and Visser, 2010; Weidtkamp-Peters and Stahl,
791 2017) were taken at the confocal laser scanning microscope FV3000 (Olympus) equipped
792 with a multi-photon counting device MultiHarp 150 (PicoQuant) with avalanche photo
793 diodes (τ-SPADs) and bandpass filter (520/35). Erythrosine B (quenched in saturated
794 potassium iodide) was used to record the Instrument Response Function to correct for the
795 time between laser pulse and detection. Calibration of the system was performed for every
796 experiment and measurements were conducted in darkness. FIT-GFP and
797 FITmSS271AA-GFP were used as negative controls (donor only), FIT-GFP or
798 FITmSS271AA-GFP (donor) and bHLH039-mCherry (acceptor) as FRET pair. GFP was

799 excited with a linearly polarized pulsed (32 MHz) 485 nm laser and 0.01-0.1 µW output
800 power. Measurements were recorded with a UPLSAPO 60XW (Olympus) objective, zoom
801 factor of 8, pixel dwell time of 12.5 µs, objective frame size of 256x256, and 60 frames.
802 Measurements were controlled with the manufacturer's FV31S-SW (Olympus) software
803 and SymPhoTime 64 (PicoQuant) software. SymPhoTime 64 (PicoQuant) software was
804 used for analysis in the respective regions of interest (whole nucleus, NB, NP) and to
805 generate color-coded fluorescence lifetime value images. Number of parameters for the
806 fit depended on the region of interest.

807 **Circularity quantification**

808 Circularity quantification was performed with the software ImageJ (National
809 Institutes of Health). Full intensity projection images were generated from Z-stacks in the
810 ZEN lite (Zeiss) software and exported as TIFF (no compression, all dimensions). Images
811 were duplicated in ImageJ and converted to RGB and 8-bit. Correct scale was set (in µm)
812 under 'Analyze' - 'Set Scale'. Threshold for the intensity limit (areas below that limit were
813 not considered for quantification) was set under 'Image' - 'Adjust' - 'Threshold' and was
814 set manually for every image. To separate the nuclear bodies better, 'Process' - 'Binary' -
815 'Watershed' was used. Parameters that should be quantified were selected under
816 'Analyze' - 'Set Measurements'. To perform the analysis, 'Analyze' - 'Analyze Particles'
817 was selected. Calculated values were further processed in Excel (Microsoft Corporation).

818 **Nuclear body quantification**

819 Nuclear body quantification was performed with the software ImageJ (National
820 Institutes of Health) and additional plugin '3D Object Counter'. Z-stacks were exported
821 from the ZEN lite (Zeiss) software as TIFF (no compression, all dimensions) first. In
822 ImageJ, Z-stacks were converted to RGB and 8-bit. Correct scale was set (in µm) under
823 'Properties'. Parameters that should be quantified were selected under 'Plugins' - '3D
824 Object Counter' - 'Set 3D Measurements'. To perform the analysis, 'Plugins' - '3D Object
825 Counter' - '3D object counter' was selected. Threshold for the intensity limit (areas below
826 that limit were not considered for quantification) was set manually for every z-stack.
827 Calculated values were further processed in Excel (Microsoft Corporation). Only size
828 between 0,01-15 μm^3 was considered.

829 **Protein domain prediction**

830 IDRs in FIT/FITmSS271AA were predicted with the tool PONDR-VLXT
831 (www.pondr.com, Molecular Kinetics, Inc.). According to the sequence of the protein, a
832 PONDR score was determined for each amino acid. A score above 0.5 indicates intrinsic
833 disorder. The bHLH domain of FIT was predicted with InterPro (www.ebi.ac.uk/interpro,
834 EMBL-EBI).

835 **Statistical analysis**

836 Line and bar diagrams represent the mean and standard deviation. Box plots show
837 25-75 percentile with min-max whiskers, mean as small square and median as line.
838 Graphs and statistical analysis were created and performed with OriginPro (OriginLab
839 Corporation). Data was tested for normal distribution with the Shapiro-Wilk test. Statistical
840 significance of data with normal distribution was tested by one-way Anova with Tukey
841 post-hoc test. Statistical significance of data with non-normal distribution was tested by
842 Mann-Whitney test. Different letters indicate statistically significant differences ($P < 0.05$).
843 Illustrations were created with BioRender.com.

844 **Accession numbers**

845 Sequence data from this article can be found in the EMBL/GenBank data libraries
846 under accession numbers*: bHLH039* (AT3G56980), *COILIN* (AT1G13030), *FIT*
847 (AT2G28160), *FRO2* (AT1G01580), *IRT1* (AT4G19690), *P15H1* (AT1G11570), *PIF3*
848 (AT1G09530), *PIF4* (AT2G43010), *PININ* (AT1G15200), *SR45* (AT1G16610), *SRm102*
849 (AT2G29210), *U2B"* (AT2G30260), *UAP56H2* (AT5G11170), and *ZAT12* (AT5G59820).

850 **Figures**

851 **Figure 1.** FIT accumulated in nuclear condensates, termed FIT nuclear bodies (NBs) in a
852 light-inducible manner, most likely following liquid-liquid phase separation (LLPS).

853 **Figure 2.** The FIT C-terminal Ser271/272 site was important for the capacity of FIT to
854 localize to NBs.

855 **Figure 3.** FIT was present in homodimeric protein complexes in NBs, dependent on
856 Ser271/272 site.

857 **Figure 4.** FIT was present in heterodimeric protein complexes with bHLH039 in NBs,
858 dependent on Ser271/272 site.

859 **Figure 5.** Two NB markers and splicing components were present in NBs (designated
860 type II), revealing the dynamics of FIT to accumulate in NBs.

861 **Figure 6.** Three NB markers and speckle components became localized in FIT NBs and
862 colocalized fully with FIT (designated type III), suggesting that FIT NBs have speckle
863 function.

864 **Figure 7.** FIT colocalized with photobody (PB) markers in distinct PBs.

865 **Figure 8.** Root iron reductase activity is promoted under blue light.

866 **Figure 9.** Induction of FIT target gene expression is enhanced under blue light.

867 **Figure 10.** Schematic summary models illustrating the dynamics of FIT NB formation,
868 suggesting that FIT NBs are related to transcriptional and posttranscriptional regulation in
869 speckles.

870 **Supplemental Data**

871 **Supplemental Figure S1.** FIT NBs induced by blue light and a standardized FIT NB
872 analysis procedure was developed to analyze the characteristics and dynamics of FIT
873 NBs. (Supports Figure 1)

874 **Supplemental Figure S2.** An intrinsically disordered region, $IDR^{Ser271/272}$, is present in the
875 FIT C-terminus and disrupted in the FITmSS271AA mutant. (Supports Figure 2, 3, and 4)

876 **Supplemental Figure S3.** FIT NBs did not colocalize with Cajal body components
877 (designated type I). (Supports Figure 5 and 6)

878 **Supplemental Figure S4.** Type II and III NB markers are similarly localized upon single
879 expression as upon co-expression with FIT, except PININ. (Supports Figure 5 and 6)

880 **Supplemental Figure S5.** PB markers are similarly localized upon single expression and
881 upon co-expression with FIT. (Supports Figure 7)

882 **Supplemental Figure S6.** Differential expression of intron retention splicing variants of
883 iron deficiency genes in response to iron deficiency and blue light. (Supports Figure 9)
884 **Supplemental Figure S7.** The variations in gene expression levels between white light
885 and blue light are consistent across both intron retention splicing variants and the overall
886 transcript pool. (Supports Figure 9 and Supplemental Figure S6)
887 **Supplemental Table S1.** List of primers used in this study.
888 **Supplemental Table S2.** List of vectors used in this study.
889 **Supplemental Movie S1.** Light induction triggers the formation of NBs with FIT and
890 FITmSS271AA with different dynamics. (Supports Figure 1 and 2)

891 **Acknowledgements**

892 We thank Elke Wieneke and Monique Eutebach (Institute of Botany, Heinrich-
893 Heine-University, Düsseldorf, Germany) for excellent technical assistance. We
894 acknowledge the contribution of the student Daniel Torno. We thank Rebecca C. Burkart
895 (Institute of Developmental Genetics, Heinrich-Heine-University, Düsseldorf, Germany),
896 Sebastian Hänsch and Stefanie Weidtkamp-Peters (Center for Advanced Imaging,
897 Heinrich-Heine-University, Düsseldorf, Germany) for help and advice with microscopy and
898 data analysis. K.T. is an associate member of the DFG-funded International Graduate
899 School for Plant Science iGRAD*plant* (IRTG 2466 "Network, exchange, and training
900 program to understand plant resource allocation"), Düsseldorf, Germany.

901 **Funding**

902 This work was funded by Deutsche Forschungsgemeinschaft (DFG, German
903 Research Foundation) under GRK F020512056 (NEXT*plant*), SFB 1208 project B05, and
904 Germany´s Excellence Strategy – EXC-2048/1 – project ID 390686111. Funding for
905 instrumentation: Zeiss ELYRA PS: DFG- INST 208/613-1 FUGG; Zeiss LSM780 + 4-
906 channel FLIM extension (Picoquant): DFG- INST 208/551-1 FUGG; Olympus FV3000
907 Confocal Laser Scanning Microscope with 4-channel FLIM extension (PicoQuant
908 rapidFLIM): DFG- INST 1358/44-1 FUGB.

909 K.T., R.I., Y.S., P.B. and T.B. designed the research; K.T. performed research;
910 K.T., R.I., Y.S., and T.B. analyzed data; R.G. contributed key materials; K.T. wrote the
911 paper; P.B. acquired funding; all authors reviewed and edited the article.

912 **References**

913 **Abdallah, H. Ben and Bauer, P.** (2016). Quantitative reverse transcription-qPCR-based
914 gene expression analysis in plants. Methods Mol. Biol. **479**: 9–24.

915 **Ali, G.S., Golovkin, M., and Reddy, A.S.N.** (2003). Nuclear localization and in vivo
916 dynamics of a plant-specific serine/arginine-rich protein. Plant J. **36**: 883–893.

917 **Bancaud, A., Huet, S., Rabut, G., and Ellenberg, J.** (2010). Fluorescence Perturbation
918 Techniques to Study Mobility and Molecular Dynamics of Proteins in Live Cells:
919 FRAP, Photoactivation, Photoconversion, and FLIP. Cold Spring Harb. Protoc.:
920 1303–1325.

921 **Bauer, D., Viczían, A., Kircher, S., Nobis, T., Nitschke, R., Kunkel, T., Panigrahi,**
922 **K.C.S., Ádám, É., Fejes, E., Schäfer, E., and Nagy, F.** (2004). Constitutive
923 Photomorphogenesis 1 and Multiple Photoreceptors Control Degradation of
924 Phytochrome Interacting Factor 3, a Transcription Factor Required for Light
925 Signaling in Arabidopsis. Plant Cell **16**: 1433–1445.

926 **Bauer, P., Ling, H.Q., and Guerinot, M. Lou** (2007). FIT, the FER-LIKE IRON
927 DEFICIENCY INDUCED TRANSCRIPTION FACTOR in Arabidopsis. Plant Physiol.
928 Biochem. **45**: 260–261.

929 **Bi, Y. et al.** (2021). Arabidopsis ACINUS is O-glycosylated and regulates transcription
930 and alternative splicing of regulators of reproductive transitions. Nat. Commun. **12**:
931 1–13.

932 **Bleckmann, A., Weidtkamp-Peters, S., Seidel, C.A.M., and Simon, R.** (2010). Stem
933 Cell Signaling in Arabidopsis Requires CRN to Localize CLV2 to the Plasma
934 Membrane. Plant Physiol. **152**: 166–176.

935 **Boija, A. et al.** (2018). Transcription Factors Activate Genes through the Phase-
936 Separation Capacity of Their Activation Domains. Cell **175**: 1842–1855.

937 **Borst, J.W. and Visser, A.J.W.G.** (2010). Fluorescence lifetime imaging microscopy in
938 life sciences. Meas. Sci. Technol. **21**: 1–21.

939 **Bracha, D., Walls, M.T., Wei, M.T., Zhu, L., Kurian, M., Avalos, J.L., Toettcher, J.E.,**
940 **and Brangwynne, C.P.** (2018). Mapping Local and Global Liquid Phase Behavior
941 in Living Cells Using Photo-Oligomerizable Seeds. Cell **175**: 1467–1480.

942 **Brodsky, S., Jana, T., Mittelman, K., Chapal, M., Kumar, D.K., Carmi, M., and**
943 **Barkai, N.** (2020). Intrinsically Disordered Regions Direct Transcription Factor In
944 Vivo Binding Specificity. Mol. Cell **79**: 459–471.

945 **Brumbarova, T. and Ivanov, R.** (2019). The Nutrient Response Transcriptional
946 Regulome of Arabidopsis. iScience **19**: 358–368.
947 **Burkart, R.C., Strotmann, V.I., Kirschner, G.K., Akinci, A., Czempik, L., Dolata, A.,**
948 **Maizel, A., Weidtkamp-Peters, S., and Stahl, Y.** (2022). PLETHORA-WOX5
949 interaction and subnuclear localization control Arabidopsis root stem cell
950 maintenance. EMBO Rep. **23**: 1–18.
951 **Van Buskirk, E.K., Reddy, A.K., Nagatani, A., and Chen, M.** (2014). Photobody
952 Localization of Phytochrome B Is Tightly Correlated with Prolonged and Light-
953 Dependent Inhibition of Hypocotyl Elongation in the Dark. Plant Physiol. **165**: 595–
954 607.
955 **Chen, D., Lyu, M., Kou, X., Li, J., Yang, Z., Gao, L., Li, Y., Fan, L., Shi, H., and**
956 **Zhong, S.** (2022). Integration of light and temperature sensing by liquid-liquid
957 phase separation of phytochrome B. Mol. Cell **82**: 1–15.
958 **Clough, S.J. and Bent, A.F.** (1998). Floral dip: a simplified method for Agrobacterium-
959 mediated transformation of Arabidopsis thaliana. Plant J. **16**: 735–743.
960 **Colangelo, E.P. and Guerinot, M. Lou** (2004). The Essential Basic Helix-Loop-Helix
961 Protein FIT1 Is Required for the Iron Deficiency Response. Plant Cell **16**: 3400–
962 3412.
963 **Collier, S., Pendle, A., Boudonck, K., van Rij, T., Dolan, L., and Shaw, P.** (2006). A
964 Distant Coilin Homologue Is Required for the Formation of Cajal Bodies in
965 Arabidopsis. Mol. Biol. Cell **17**: 2942–2951.
966 **Cui, Y., Chen, C.L., Cui, M., Zhou, W.J., Wu, H.L., and Ling, H.Q.** (2018). Four IVa
967 bHLH Transcription Factors Are Novel Interactors of FIT and Mediate JA Inhibition
968 of Iron Uptake in Arabidopsis. Mol. Plant **11**: 1166–1183.
969 **Eide, D., Broderius, M., Fett, J., and Guerinot, M. Lou** (1996). A novel iron-regulated
970 metal transporter from plants identified by functional expression in yeast. Proc. Natl.
971 Acad. Sci. **93**: 5624–5628.
972 **Emenecker, R.J., Holehouse, A.S., and Strader, L.C.** (2020). Emerging Roles for
973 Phase Separation in Plants. Dev. Cell **55**: 69–83.
974 **Emenecker, R.J., Holehouse, A.S., and Strader, L.C.** (2021). Sequence determinants
975 of in cell condensate morphology, dynamics, and oligomerization as measured by
976 number and brightness analysis. Cell Commun. Signal. **19**: 1–15.
977 **Fanara, S., Schloesser, M., Hanikenne, M., and Motte, P.** (2022). Altered metal

978 distribution in the sr45-1 Arabidopsis mutant causes developmental defects. Plant J.
979 **110**: 1332–1352.
980 **Fang, X., Wang, L., Ishikawa, R., Li, Y., Fiedler, M., Liu, F., Calder, G., Rowan, B.,**
981 **Weigel, D., Li, P., and Dean, C.** (2019). Arabidopsis FLL2 promotes liquid–liquid
982 phase separation of polyadenylation complexes. Nature **569**: 265–269.
983 **Galganski, L., Urbanek, M.O., and Krzyzosiak, W.J.** (2017). Nuclear speckles:
984 Molecular organization, biological function and role in disease. Nucleic Acids Res.
985 **45**: 10350–10368.
986 **Gao, F., Robe, K., Bettembourg, M., Navarro, N., Rofidal, V., Santoni, V., Gaymard,**
987 **F., Vignols, F., Roschzttardtz, H., Izquierdo, E., and Dubos, C.** (2020). The
988 Transcription Factor bHLH121 Interacts with bHLH105 (ILR3) and Its Closest
989 Homologs to Regulate Iron Homeostasis in Arabidopsis. Plant Cell **32**: 508–524.
990 **Gao, Y.-Q., Bu, L.-H., Han, M.-L., Wang, Y.-L., Li, Z.-Y., Liu, H.-T., and Chao, D.-Y.**
991 (2021). Long-distance blue light signalling regulates phosphate deficiency-induced
992 primary root growth inhibition. Mol. Plant **14**: 1–15.
993 **Gratz, R. et al.** (2019). CIPK11-Dependent Phosphorylation Modulates FIT Activity to
994 Promote Arabidopsis Iron Acquisition in Response to Calcium Signaling. Dev. Cell
995 **48**: 726–740.
996 **Gratz, R., Brumbarova, T., Ivanov, R., Trofimov, K., Tünnermann, L., Ochoa-**
997 **Fernandez, R., Blomeier, T., Meiser, J., Weidtkamp-Peters, S., Zurbriggen, M.,**
998 **and Bauer, P.** (2020). Phospho-mutant activity assays provide evidence for
999 alternative phospho-regulation pathways of the transcription factor FER-LIKE IRON
1000 DEFICIENCY-INDUCED TRANSCRIPTION FACTOR. New Phytol. **225**: 250–267.
1001 **Guo, Z., Xu, J., Wang, Y., Hu, C., Shi, K., Zhou, J., Xia, X., Zhou, Y., Foyer, C.H., and**
1002 **Yu, J.** (2021). The phyB-dependent induction of HY5 promotes iron uptake by
1003 systemically activating FER expression. EMBO Rep. **22**: 1–15.
1004 **Huang, X., Xiao, N., Zou, Y., Xie, Y., Tang, L., Zhang, Y., Yu, Y., Li, Y., and Xu, C.**
1005 (2022). Heterotypic transcriptional condensates formed by prion-like paralogous
1006 proteins canalize flowering transition in tomato. Genome Biol. **23**: 1–21.
1007 **Jakoby, M., Wang, H.Y., Reidt, W., Weisshaar, B., and Bauer, P.** (2004). FRU
1008 (BHLH029) is required for induction of iron mobilization genes in Arabidopsis
1009 thaliana. FEBS Lett. **577**: 528–534.
1010 **Jung, J.-H. et al.** (2020). A prion-like domain in ELF3 functions as a thermosensor in

1011 Arabidopsis. Nature **585**: 256–260.
1012 **Kaiserli, E., Páldi, K., O'Donnell, L., Batalov, O., Pedmale, U. V., Nusinow, D.A.,**
1013 **Kay, S.A., and Chory, J.** (2015). Integration of Light and Photoperiodic Signaling in
1014 Transcriptional Nuclear Foci. Dev. Cell **35**: 311–321.
1015 **Kalinina, N.O., Makarova, S., Makhotenko, A., Love, A.J., and Taliansky, M.** (2018).
1016 The Multiple Functions of the Nucleolus in Plant Development, Disease and Stress
1017 Responses. Front. Plant Sci. **9**: 1–19.
1018 **Kammel, C., Thomaier, M., Sørensen, B.B., Schubert, T., Längst, G., Grasser, M.,**
1019 **and Grasser, K.D.** (2013). Arabidopsis DEAD-Box RNA Helicase UAP56 Interacts
1020 with Both RNA and DNA as well as with mRNA Export Factors. PLoS One **8**: 1–12.
1021 **Kanwar, P., Baby, D., and Bauer, P.** (2021). Interconnection of iron and osmotic stress
1022 signalling in plants: is FIT a regulatory hub to cross-connect abscisic acid
1023 responses? Plant Biol. **23**: 31–38.
1024 **Kim, D.W., Jeon, S.J., Hwang, S.M., Hong, J.C., and Bahk, J.D.** (2016). The C3H-
1025 type zinc finger protein GDS1/C3H42 is a nuclear-speckle-localized protein that is
1026 essential for normal growth and development in Arabidopsis. Plant Sci. **250**: 141–
1027 153.
1028 **Kim, S.A., Lacroix, I.S., Gerber, S.A., and Guerinot, M. Lou** (2019). The iron
1029 deficiency response in Arabidopsis thaliana requires the phosphorylated
1030 transcription factor URI. Proc. Natl. Acad. Sci. **116**: 24933–24942.
1031 **Kircher, S., Gil, P., Kozma-Bognár, L., Fejes, E., Speth, V., Husselstein-Muller, T.,**
1032 **Bauer, D., Ádám, É., Schäfer, E., and Nagy, F.** (2002). Nucleocytoplasmic
1033 Partitioning of the Plant Photoreceptors Phytochrome A, B, C, D, and E Is
1034 Regulated Differentially by Light and Exhibits a Diurnal Rhythm. Plant Cell **14**:
1035 1541–1555.
1036 **Korshunova, Y.O., Eide, D., Clark, W.G., Guerinot, M. Lou, and Himadri, B.** (1999).
1037 The IRT1 protein from Arabidopsis thaliana is a metal transporter with a broad
1038 substrate range. Plant Mol. Biol. **40**: 37–44.
1039 **Lafontaine, D.L.J., Riback, J.A., Bascetin, R., and Brangwynne, C.P.** (2021). The
1040 nucleolus as a multiphase liquid condensate. Nat. Rev. Mol. Cell Biol. **22**: 165–182.
1041 **Lampropoulos, A., Sutikovic, Z., Wenzl, C., Maegele, I., Lohmann, J.U., and Forner,**
1042 **J.** (2013). GreenGate - A Novel, Versatile, and Efficient Cloning System for Plant
1043 Transgenesis. PLoS One **8**: 1–15.

1044 **Le, C.T.T., Brumbarova, T., Ivanov, R., Stoof, C., Weber, E., Mohrbacher, J., Fink-**
1045 **Straube, C., and Bauer, P.** (2016). ZINC FINGER OF ARABIDOPSIS
1046 THALIANA12 (ZAT12) Interacts with FER-LIKE IRON DEFICIENCY-INDUCED
1047 TRANSCRIPTION FACTOR (FIT) Linking Iron Deficiency and Oxidative Stress
1048 Responses. Plant Physiol. **170**: 540–557.
1049 **Legris, M., Klose, C., Burgie, E.S., Rojas, C.C., Neme, M., Hiltbrunner, A., Wigge,**
1050 **P.A., Schäfer, E., Vierstra, R.D., and Casaj, J.J.** (2016). Phytochrome B
1051 integrates light and temperature signals in Arabidopsis. Science (80-.). **354**: 897–
1052 900.
1053 **Leivar, P. and Monte, E.** (2014). PIFs: Systems Integrators in Plant Development. Plant
1054 Cell **26**: 56–78.
1055 **Leonelli, L., Erickson, E., Lyska, D., and Niyogi, K.K.** (2016). Transient expression in
1056 Nicotiana benthamiana for rapid functional analysis of genes involved in non-
1057 photochemical quenching and carotenoid biosynthesis. Plant J. **88**: 375–386.
1058 **Li, S., Yamada, M., Han, X., Ohler, U., and Benfey, P.N.** (2016a). High-Resolution
1059 Expression Map of the Arabidopsis Root Reveals Alternative Splicing and lincRNA
1060 Regulation. Dev. Cell **39**: 508–522.
1061 **Li, W., Lin, W.-D., Ray, P., Lan, P., and Schmidt, W.** (2013). Genome-Wide Detection
1062 of Condition-Sensitive Alternative Splicing in Arabidopsis Roots. Plant Physiol. **162**:
1063 1750–1763.
1064 **Li, X., Zhang, H., Ai, Q., Liang, G., and Yu, D.** (2016b). Two bHLH Transcription
1065 Factors, bHLH34 and bHLH104, Regulate Iron Homeostasis in Arabidopsis
1066 thaliana. Plant Physiol. **170**: 2478–2493.
1067 **Liang, G., Zhang, H., Li, X., Ai, Q., and Yu, D.** (2017). bHLH transcription factor
1068 bHLH115 regulates iron homeostasis in Arabidopsis thaliana. J. Exp. Bot. **68**:
1069 1743–1755.
1070 **Lin, C.L., Leu, S., Lu, M.C., and Ouyang, P.** (2004). Over-expression of SR-cyclophilin,
1071 an interaction partner of nuclear pinin, releases SR family splicing factors from
1072 nuclear speckles. Biochem. Biophys. Res. Commun. **321**: 638–647.
1073 **Lingam, S., Mohrbacher, J., Brumbarova, T., Potuschak, T., Fink-Straube, C.,**
1074 **Blondet, E., Genschik, P., and Bauer, P.** (2011). Interaction between the bHLH
1075 Transcription Factor FIT and ETHYLENE INSENSITIVE3/ETHYLENE
1076 INSENSITIVE3-LIKE1 Reveals Molecular Linkage between the Regulation of Iron

1077 Acquisition and Ethylene Signaling in Arabidopsis. Plant Cell **23**: 1815–1829.
1078 **Lorković, Z.J., Hilscher, J., and Barta, A.** (2008). Co-localisation studies of
1079 Arabidopsis SR splicing factors reveal different types of speckles in plant cell nuclei.
1080 Exp. Cell Res. **314**: 3175–3186.
1081 **Lorković, Z.J., Hilscher, J., and Barta, A.** (2004). Use of Fluorescent Protein Tags to
1082 Study Nuclear Organization of the Spliceosomal Machinery in Transiently
1083 Transformed Living Plant Cells. Mol. Biol. Cell **15**: 3233–3243.
1084 **Love, A.J., Yu, C., Petukhova, N. V., Kalinina, N.O., Chen, J., and Taliansky, M.E.**
1085 (2017). Cajal bodies and their role in plant stress and disease responses. RNA Biol.
1086 **14**: 779–790.
1087 **Mankotia, S., Singh, D., Monika, K., Kalra, M., Meena, H., Meena, V., Yadav, R.K.,**
1088 **Pandey, A.K., and Satbhai, S.B.** (2023). ELONGATED HYPOCOTYL 5 regulates
1089 BRUTUS and affects iron acquisition and homeostasis in Arabidopsis thaliana.
1090 Plant J.: 1–18.
1091 **Martin, K., Kopperud, K., Chakrabarty, R., Banerjee, R., Brooks, R., and Goodin,**
1092 **M.M.** (2009). Transient expression in Nicotiana benthamiana fluorescent marker
1093 lines provides enhanced definition of protein localization, movement and
1094 interactions in planta. Plant J. **59**: 150–162.
1095 **Meiser, J., Lingam, S., and Bauer, P.** (2011). Posttranslational Regulation of the Iron
1096 Deficiency Basic Helix-Loop-Helix Transcription Factor FIT Is Affected by Iron and
1097 Nitric Oxide. Plant Physiol. **157**: 2154–2166.
1098 **Meyer, H.M.** (2020). In search of function: nuclear bodies and their possible roles as
1099 plant environmental sensors. Curr. Opin. Plant Biol. **58**: 33–40.
1100 **Mikulski, P., Wolff, P., Lu, T., Nielsen, M., Echevarria, E.F., Zhu, D., Questa, J.I.,**
1101 **Saalbach, G., Martins, C., and Dean, C.** (2022). VAL1 acts as an assembly
1102 platform co-ordinating co-transcriptional repression and chromatin regulation at
1103 Arabidopsis FLC. Nat. Commun. **13**: 1–12.
1104 **Ni, M., Tepperman, J.M., and Quail, P.H.** (1998). PIF3, a Phytochrome-Interacting
1105 Factor Necessary for Normal Photoinduced Signal Transduction, Is a Novel Basic
1106 Helix-Loop-Helix Protein. Cell **95**: 657–667.
1107 **Oh, E., Kim, J., Park, E., Kim, J.-I., Kang, C., and Choi, G.** (2004). PIL5, a
1108 Phytochrome-Interacting Basic Helix-Loop-Helix Protein, Is a Key Negative
1109 Regulator of Seed Germination in Arabidopsis thaliana. Plant Cell **16**: 3045–3058.

1110 **Owen, I. and Shewmaker, F.** (2019). The Role of Post-Translational Modifications in
1111 the Phase Transitions of Intrinsically Disordered Proteins. Int. J. Mol. Sci. **20**: 1–14.
1112 **Pardi, S.A. and Nusinow, D.A.** (2021). Out of the Dark and Into the Light: A New View
1113 of Phytochrome Photobodies. Front. Plant Sci. **12**: 1–15.
1114 **Pedmale, U. V., Huang, S.-S.C., Zander, M., Cole, B.J., Hetzel, J., Ljung, K., Reis,**
1115 **P.A.B., Sridevi, P., Nito, K., Nery, J.R., Ecker, J.R., and Chory, J.** (2016).
1116 Cryptochromes Interact Directly with PIFs to Control Plant Growth in Limiting Blue
1117 Light. Cell **164**: 233–245.
1118 **Pendle, A.F., Cark, G.P., Boon, R., Lewandowska, D., Lam, Y.W., Andersen, J.,**
1119 **Mann, M., Lamond, A.I., Brown, J.W.S., and Shaw, P.J.** (2005). Proteomic
1120 Analysis of the Arabidopsis Nucleolus Suggests Novel Nucleolar Functions. Mol.
1121 Biol. Cell **16**: 260–269.
1122 **Pham, V.N., Kathare, P.K., and Huq, E.** (2018). Phytochromes and Phytochrome
1123 Interacting Factors. Plant Physiol. **176**: 1025–1038.
1124 **Powers, S.K. et al.** (2019). Nucleo-cytoplasmic Partitioning of ARF Proteins Controls
1125 Auxin Responses in Arabidopsis thaliana. Mol. Cell **76**: 177–190.
1126 **Qiu, Y., Li, M., Kim, R.J.A., Moore, C.M., and Chen, M.** (2019). Daytime temperature is
1127 sensed by phytochrome B in Arabidopsis through a transcriptional activator
1128 HEMERA. Nat. Commun. **10**: 1–13.
1129 **Qiu, Y., Pasoreck, E.K., Yoo, C.Y., He, J., Wang, H., Bajracharya, A., Li, M., Larsen,**
1130 **H.D., Cheung, S., and Chen, M.** (2021). RCB initiates Arabidopsis
1131 thermomorphogenesis by stabilizing the thermoregulator PIF4 in the daytime. Nat.
1132 Commun. **12**: 1–13.
1133 **Reddy, A.S.N., Day, I.S., Gohring, J., and Barta, A.** (2012). Localization and Dynamics
1134 of Nuclear Speckles in Plants. Plant Physiol. **158**: 67–77.
1135 **Riback, J.A., Zhu, L., Ferrolino, M.C., Tolbert, M., Mitrea, D.M., Sanders, D.W., Wei,**
1136 **M.-T., Kriwacki, R.W., and Brangwynne, C.P.** (2020). Composition-dependent
1137 thermodynamics of intracellular phase separation. Nature **581**: 209–214.
1138 **Robinson, N.J., Procter, C.M., Connolly, E.L., and Guerinot, M. Lou** (1999). A ferric-
1139 chelate reductase for iron uptake from soils. Nature **397**: 694–697.
1140 **Römheld, V. and Marschner, H.** (1986). Mobilization of iron in the rhizosphere of
1141 different plant species. Adv. Plant Nutr. **2**: 155–204.
1142 **Salladini, E., Jørgensen, M.L.M., Theisen, F.F., and Skriver, K.** (2020). Intrinsic

1143 Disorder in Plant Transcription Factor Systems: Functional Implications. Int. J. Mol.
1144 Sci. **21**: 1–35.
1145 **Salomé, P.A., Oliva, M., Weigel, D., and Krämer, U.** (2013). Circadian clock
1146 adjustment to plant iron status depends on chloroplast and phytochrome function.
1147 EMBO J. **32**: 511–523.
1148 **Santi, S. and Schmidt, W.** (2009). Dissecting iron deficiency-induced proton extrusion
1149 in Arabidopsis roots. New Phytol. **183**: 1072–1084.
1150 **Schwarz, B. and Bauer, P.** (2020). FIT, a regulatory hub for iron deficiency and stress
1151 signaling in roots, and FIT-dependent and -independent gene signatures. J. Exp.
1152 Bot. **71**: 1694–1705.
1153 **Shamloul, M., Trusa, J., Mett, V., and Yusibov, V.** (2014). Optimization and Utilization
1154 of Agrobacterium-mediated Transient Protein Production in Nicotiana. J. Vis. Exp.
1155 **86**: 1–13.
1156 **Shin, Y., Berry, J., Pannucci, N., Haataja, M.P., Toettcher, J.E., and Brangwynne,**
1157 **C.P.** (2017). Spatiotemporal Control of Intracellular Phase Transitions Using Light-
1158 Activated optoDroplets. Cell **168**: 159–171.
1159 **Stahl, Y. et al.** (2013). Moderation of Arabidopsis root Stemness by CLAVATA1 and
1160 ARABIDOPSIS CRINKLY4 Receptor Kinase Complexes. Curr. Biol. **23**: 362–371.
1161 **Strader, L., Weijers, D., and Wagner, D.** (2022). Plant transcription factors - being in
1162 the right place with the right company. Curr. Opin. Plant Biol. **65**: 1–8.
1163 **Tarczewska, A. and Greb-Markiewicz, B.** (2019). The Significance of the Intrinsically
1164 Disordered Regions for the Functions of the bHLH Transcription Factors. Int. J. Mol.
1165 Sci. **20**: 1–20.
1166 **Trinkle-Mulcahy, L. and Sleeman, J.E.** (2017). The Cajal body and the nucleolus: “In a
1167 relationship” or “It’s complicated”? RNA Biol. **14**: 739–751.
1168 **Trofimov, K., Ivanov, R., Eutebach, M., Acaroglu, B., Mohr, I., Bauer, P., and**
1169 **Brumbarova, T.** (2019). Mobility and localization of the iron deficiency-induced
1170 transcription factor bHLH039 change in the presence of FIT. Plant Direct **3**: 1–11.
1171 **Vert, G.A., Briat, J.F., and Curie, C.** (2003). Dual Regulation of the Arabidopsis High-
1172 Affinity Root Iron Uptake System by Local and Long-Distance Signals. Plant
1173 Physiol. **132**: 796–804.
1174 **Wang, B., Zhang, H., Huai, J., Peng, F., Wu, J., Lin, R., and Fang, X.** (2022).
1175 Condensation of SEUSS promotes hyperosmotic stress tolerance in Arabidopsis.

1176 Nat. Chem. Biol. **18**: 1361–1369.
1177 **Wang, N., Cui, Y., Liu, Y., Fan, H., Du, J., Huang, Z., Yuan, Y., Wu, H., and Ling,**
1178 **H.Q.** (2013). Requirement and Functional Redundancy of Ib Subgroup bHLH
1179 Proteins for Iron Deficiency Responses and Uptake in Arabidopsis thaliana. Mol.
1180 Plant **6**: 503–513.
1181 **Wang, X., Jiang, B., Gu, L., Chen, Y., Mora, M., Zhu, M., Noory, E., Wang, Q., and**
1182 **Lin, C.** (2021). A photoregulatory mechanism of the circadian clock in Arabidopsis.
1183 Nat. Plants **7**: 1397–1408.
1184 **Wedepohl, K.H.** (1995). The composition of the continental crust. Geochim.
1185 Cosmochim. Acta **59**: 1217–1232.
1186 **Weidtkamp-Peters, S., Rehwald, S., and Stahl, Y.** (2022). Homo-FRET Imaging to
1187 Study Protein–Protein Interaction and Complex Formation in Plants. In Plant
1188 Synthetic Biology: Methods and Protocols, M.D. Zurbriggen, ed (Springer US: New
1189 York, NY), pp. 197–208.
1190 **Weidtkamp-Peters, S. and Stahl, Y.** (2017). The Use of FRET/FLIM to Study Proteins
1191 Interacting with Plant Receptor Kinases. In Plant Receptor Kinases: Methods and
1192 Protocols, R.B. Aalen, ed (Springer New York: New York, NY), pp. 163–175.
1193 **Wild, M., Davière, J.M., Regnault, T., Sakvarelidze-Achard, L., Carrera, E., Lopez**
1194 **Diaz, I., Cayrel, A., Dubeaux, G., Vert, G., and Achard, P.** (2016). Tissue-Specific
1195 Regulation of Gibberellin Signaling Fine-Tunes Arabidopsis Iron-Deficiency
1196 Responses. Dev. Cell **37**: 190–200.
1197 **Yang, Y., Ou, B., Zhang, J., Si, W., Gu, H., Qin, G., and Qu, L.-J.** (2014). The
1198 Arabidopsis Mediator subunit MED16 regulates iron homeostasis by associating
1199 with EIN3/EIL1 through subunit MED25. Plant J. **77**: 838–851.
1200 **Yi, Y. and Guerinot, M. Lou** (1996). Genetic evidence that induction of root Fe(III)
1201 chelate reductase activity is necessary for iron uptake under iron deficiency. Plant J.
1202 **10**: 835–844.
1203 **Yuan, Y., Wu, H., Wang, N., Li, J., Zhao, W., Du, J., Wang, D., and Ling, H.Q.** (2008).
1204 FIT interacts with AtbHLH38 and AtbHLH39 in regulating iron uptake gene
1205 expression for iron homeostasis in Arabidopsis. Cell Res. **18**: 385–397.
1206 **Yuan, Y.X., Zhang, J., Wang, D.W., and Ling, H.Q.** (2005). AtbHLH29 of Arabidopsis
1207 thaliana is a functional ortholog of tomato FER involved in controlling iron
1208 acquisition in strategy I plants. Cell Res. **15**: 613–621.

1209 **Zhang, J., Liu, B., Li, M., Feng, D., Jin, H., Wang, P., Liu, J., Xiong, F., Wang, J., and**
1210 **Wang, H.** (2015). The bHLH Transcription Factor bHLH104 Interacts with IAA-
1211 LEUCINE RESISTANT3 and Modulates Iron Homeostasis in Arabidopsis. Plant Cell
1212 **27**: 787–805.
1213 **Zhang, Y., Wu, H., Wang, N., Fan, H., Chen, C., Cui, Y., Liu, H., and Ling, H.-Q.**
1214 (2014). Mediator subunit 16 functions in the regulation of iron uptake gene
1215 expression in Arabidopsis. New Phytol. **203**: 770–783.
1216 **Zhu, P., Lister, C., and Dean, C.** (2021). Cold-induced Arabidopsis FRIGIDA nuclear
1217 condensates for FLC repression. Nature **599**: 657–661.
1218

Figure 1

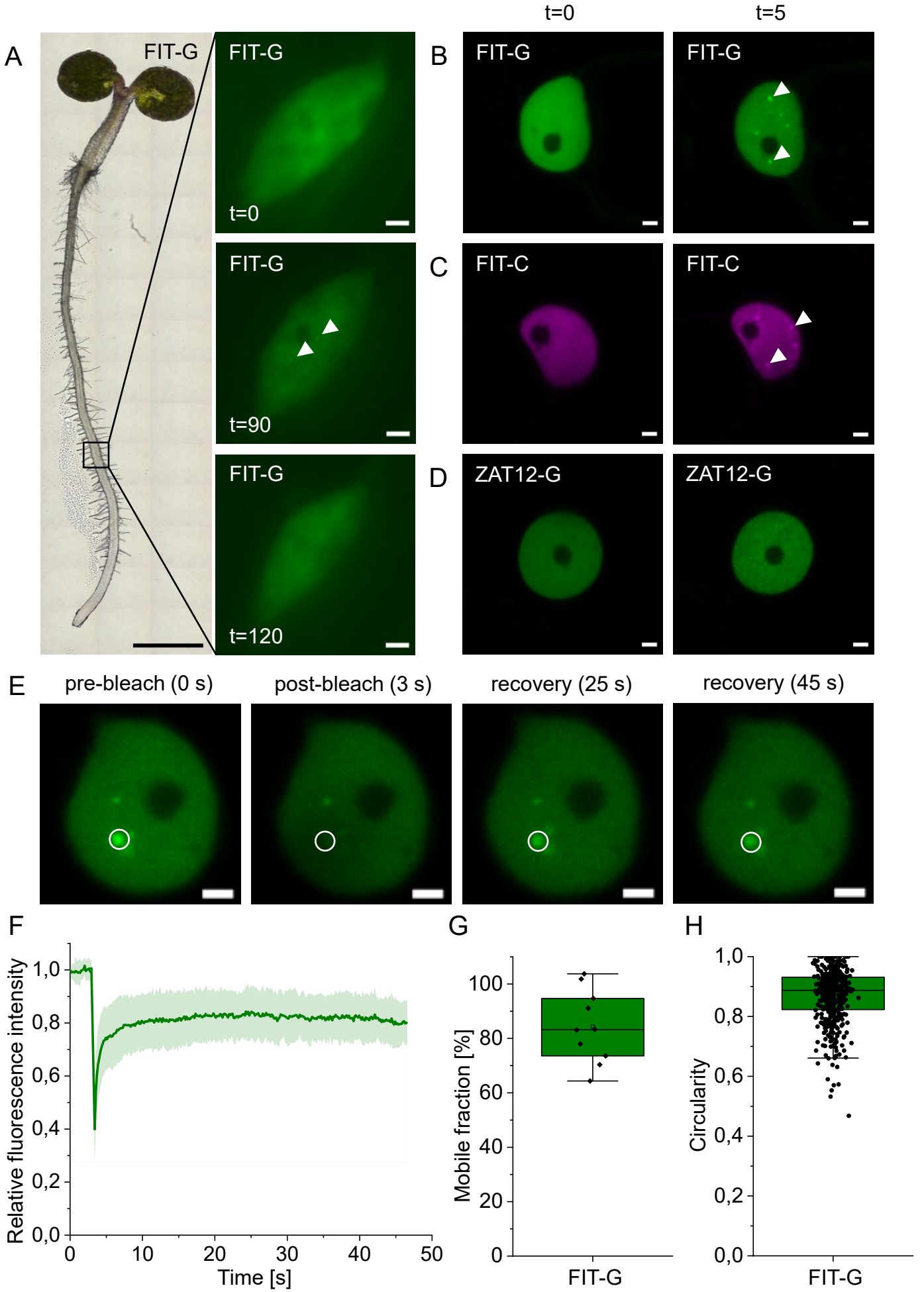
A
FIT-G
FIT-G
t=0
FIT-G
t=90
FIT-G
t=120
B
t=0
t=5
FIT-G
FIT-G
C
FIT-C
FIT-C
D
ZAT12-G
ZAT12-G
E
pre-bleach (0 s)
post-bleach (3 s)
recovery (25 s)
recovery (45 s)
F
Relative fluorescence intensity
1,0
0,8
0,6
0,4
0,2
0,0
0
10
20
30
40
50
Time [s]
G
Mobile fraction [%]
100
80
60
40
20
0
FIT-G
H
Circularity
1,0
0,8
0,6
0,4
0,2
0,0
FIT-G

Figure 1: FIT accumulated in nuclear condensates, termed FIT nuclear bodies (NBs) in a light-inducible manner, most likely following liquid-liquid phase separation (LLPS).

A, Induction of FIT NBs in Arabidopsis root epidermis cells of the root differentiation zone. Left, light microscopy overview image of a 5-d-old Arabidopsis seedling (proFIT:FIT-GFP) grown under iron deficiency. Right, nuclear localization of FIT-GFP in the root epidermis cells as indicated in the overview image, at t=0, t=90, and t=120 min. FIT-GFP signals were evenly distributed in the nucleus at t=0 min, and after induction by excitation with 488 nm laser NB formation accumulated in NBs at t=90 min, but also disappeared as shown at t=120 min. Note that root epidermis cells developed few NBs, sometimes taking up to two hours to appear. Three independent experiments with three plants were conducted. In the indicated region of interest, approximately 3-10 nuclei of 20 examined nuclei of the root epidermis cells showed NBs. A representative image from one nucleus is shown. B-D, Fluorescence protein analysis in transiently transformed *N. benthamiana* leaf epidermis cells. Confocal images of B, FIT-GFP, C, FIT-mCherry, and D, ZAT12-GFP at t=0 and t=5 min. At t=0 min, FIT-GFP and FIT-mCherry showed an even distribution within the nucleus. Following a 488 nm laser excitation, numerous NBs were clearly visible in all examined transformed cells at t=5 min. These NBs were termed FIT NBs. Under the same imaging conditions, ZAT12-GFP did not show NB formation. According to these results, a standardized FIT NB analysis procedure was set up (**Supplemental Figure S1C**). See also **Supplemental Movie S1A-C**. Representative images from two to three independent experiments. E-G, FRAP measurements to test for liquid-like behavior of FIT NBs, using the standardized FIT NB analysis procedure in transiently transformed *N. benthamiana* leaf epidermis cells. E, Representative images of the fluorescent signal during a FRAP experiment, taken before bleaching (0 s) and recovery of fluorescence at three time points after bleaching from 3 s to 45 s within the circled region of a NB. F, Line diagram representing the relative fluorescence during a FRAP measurement for 10 NBs, showing a high fluorescence recovery rate of FIT-GFP within NBs. Dark green line, mean value; light green filled area, variation. G, Box plot diagram representing the mobile fraction of FIT-GFP calculated based on the relative fluorescence recovery in F. The diagram indicates high mobility of FIT. The mean was calculated from 10 NBs from 10 nuclei from a transformed plant. Three independent experiments were conducted, one representative result is shown. H, Box plot diagram representing quantification of the FIT NB shape with the software ImageJ (National Institutes of Health), indicating that FIT NBs have circular shape. Mobility and circularity characteristics indicate that FIT NBs are most likely liquid condensates that are the result of LLPS. The mean was calculated from all NBs visible in 15 nuclei from a transformed plant. Two independent experiments were conducted, one representative result is shown.

Box plots show 25-75 percentile with min-max whiskers, mean as small square and median as line. Scale bars of nuclei images, 2 µm; scale bar full seedling, 1 mm. Arrowheads indicate NBs. G = GFP; C = mCherry.

Figure 2

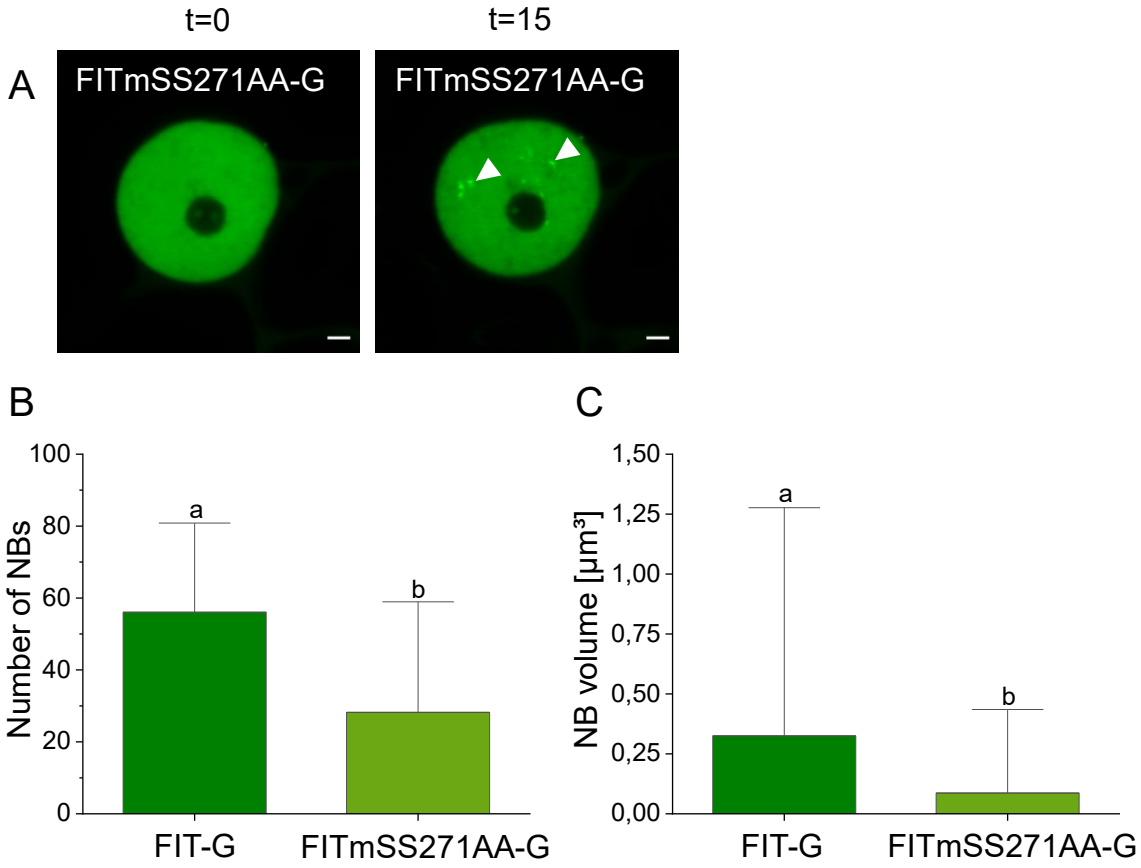
t=0
t=15
A
FITmSS271AA-G
FITmSS271AA-G
B
Number of NBs
100
80
60
40
20
0
a
b
FIT-G
FITmSS271AA-G
C
NB volume [µm³]
1,50
1,25
1,00
0,75
0,50
0,25
0,00
a
b
FIT-G
FITmSS271AA-G

Figure 2: The FIT C-terminal Ser271/272 site was important for the capacity of FIT to localize to NBs.

A, Confocal images of nuclear localization of FITmSS271AA-GFP at t=0 and t=15 min. FITmSS271AA-GFP accumulated in NBs, but NB formation required a longer time compared to FIT-GFP. See also **Supplemental Movie S1, A and C**. Two independent experiments. Representative images from one nucleus. B, Bar diagrams showing in B, number of NBs, and in C, the sizes of NBs with FIT-GFP and FITmSS271AA-GFP at t=5/15 min. NB number and size were determined with the software ImageJ (National Institute of Health). FIT-GFP accumulated in more and larger NBs than FITmSS271AA-GFP. See **Supplemental Movie S1, A and C**. FITmSS271AA-GFP lacks $IDR^{Ser271/272}$. This IDR may be relevant for FIT NB formation (**Supplemental Figure S2**). In B and C, bar diagrams represent the mean and standard deviation for a quantification of 15 nuclei from a transformed plant (n = 15). Two experiments were conducted, one representative result is shown.

Statistical analysis was performed with the Mann-Whitney test. Different letters indicate statistically significant differences ($P < 0.05$). Scale bar: 2 µm. Arrowheads indicate NBs. G = GFP. Analysis was conducted in transiently transformed *N. benthamiana* leaf epidermis cells, following the standardized FIT NB analysis procedure.

Figure 3

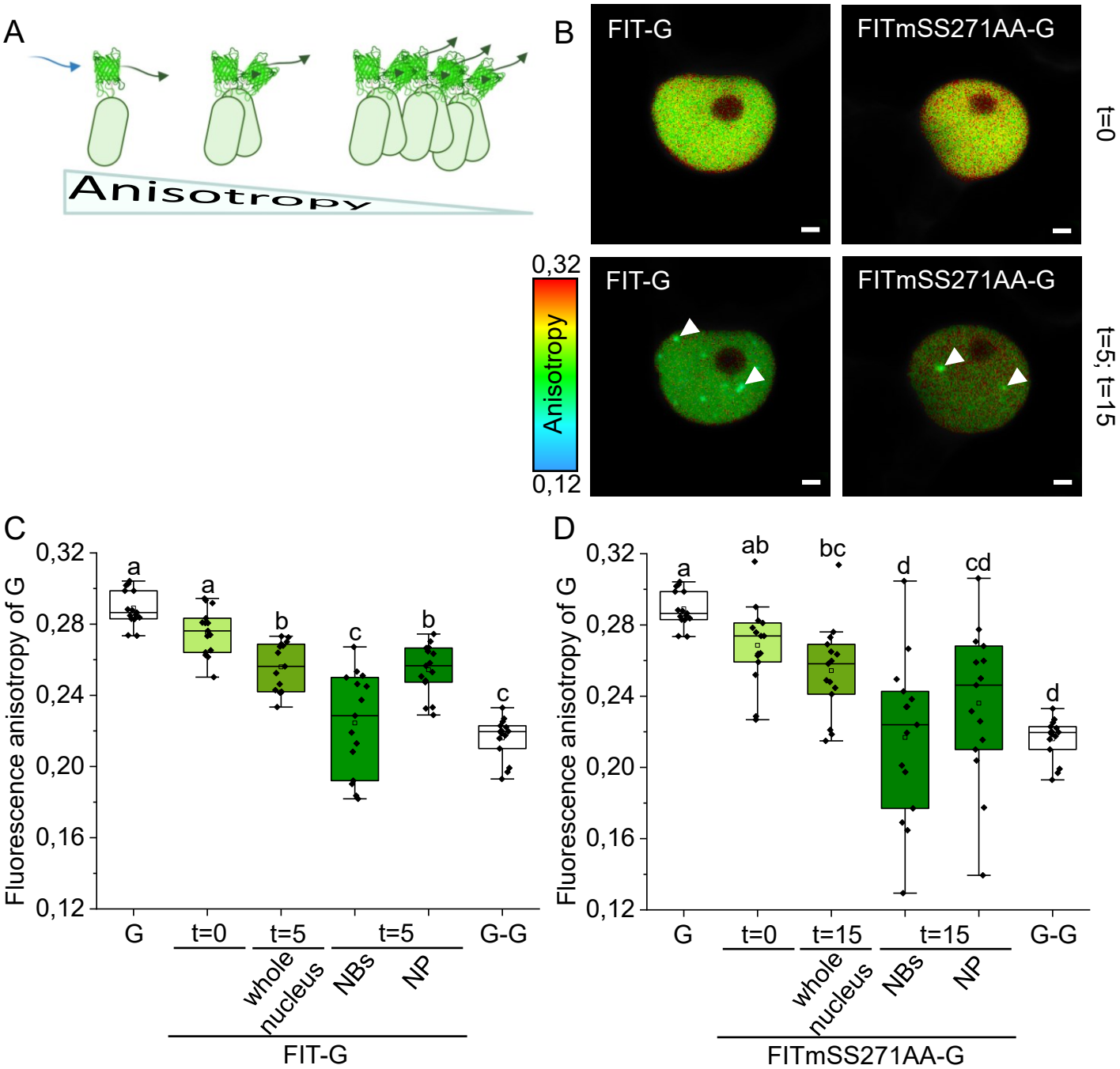
A
Anisotropy
B
FIT-G
FITmSS271AA-G
t=0
0,32
Anisotropy
0,12
FIT-G
FITmSS271AA-G
t=5; t=15
C
Fluorescence anisotropy of G
0,32
0,28
0,24
0,20
0,16
0,12
a
a
b
c
b
c
G
t=0
t=5
t=5
G-G
whole nucleus
NBs
NP
FIT-G
D
Fluorescence anisotropy of G
0,32
0,28
0,24
0,20
0,16
0,12
a
ab
bc
d
cd
d
G
t=0
t=15
t=15
G-G
whole nucleus
NBs
NP
FITmSS271AA-G

Figure 3: FIT was present in homodimeric protein complexes in NBs, dependent on Ser271/272 site.

Anisotropy (or homo-FRET) measurements of FIT-GFP and FITmSS271AA-GFP to determine homodimerization strength. A, Schematic illustration of the anisotropy principle. Energy transfer between the same kind of fluorescently tagged proteins leads to depolarization of the emitted light. Extent of the depolarization gives a hint on dimerization and oligomerization of a protein as the fluorescence anisotropy (FA) value decreases. B, Representative images showing color-coded FA values of FIT-GFP and FITmSS271AA at t=0 and t=5/15 min. C-D, Box plots representing quantification of FA values. FA was measured at t=0 within the whole nucleus and at t =5/15 min within the whole nucleus, in NBs and in residual NP. Free GFP and GFP-GFP served as references for mono- and dimerization. FA values for C, FIT-GFP, and D, FITmSS271AA-GFP. In C and D, FA values were calculated from 10-15 nuclei from a transformed plant (n = 10-15). Two experiments were conducted, one representative result is shown. C and D show the same free GFP and GFP-GFP references because both measurements were performed on the same day. FA values decreased for FIT-GFP, but not FITmSS271AA-GFP, in the whole nucleus (compare t=0 with t=5/15 min). FA values were also lowered in NBs versus NP in the case of FIT-GFP but not FITmSS271AA-GFP (compare t=5/15 min of NBs and NP). This indicates stronger homodimerization of FIT than FITmSS271AA-GFP in the whole nucleus and in NBs. $IDR^{Ser271/272}$ may therefore be relevant for FIT NB formation and FIT homodimerization (**Supplemental Figure S2**).

Box plots show 25-75 percentile with min-max whiskers, mean as small square and median as line. Statistical analysis was performed with one-way ANOVA and Tukey post-hoc test. Different letters indicate statistically significant differences ($P < 0.05$). Scale bar: 2 µm. Arrowheads indicate NBs. G = GFP. Fluorescence protein analysis was conducted in transiently transformed *N. benthamiana* leaf epidermis cells, following the standardized FIT NB analysis procedure.

Figure 4

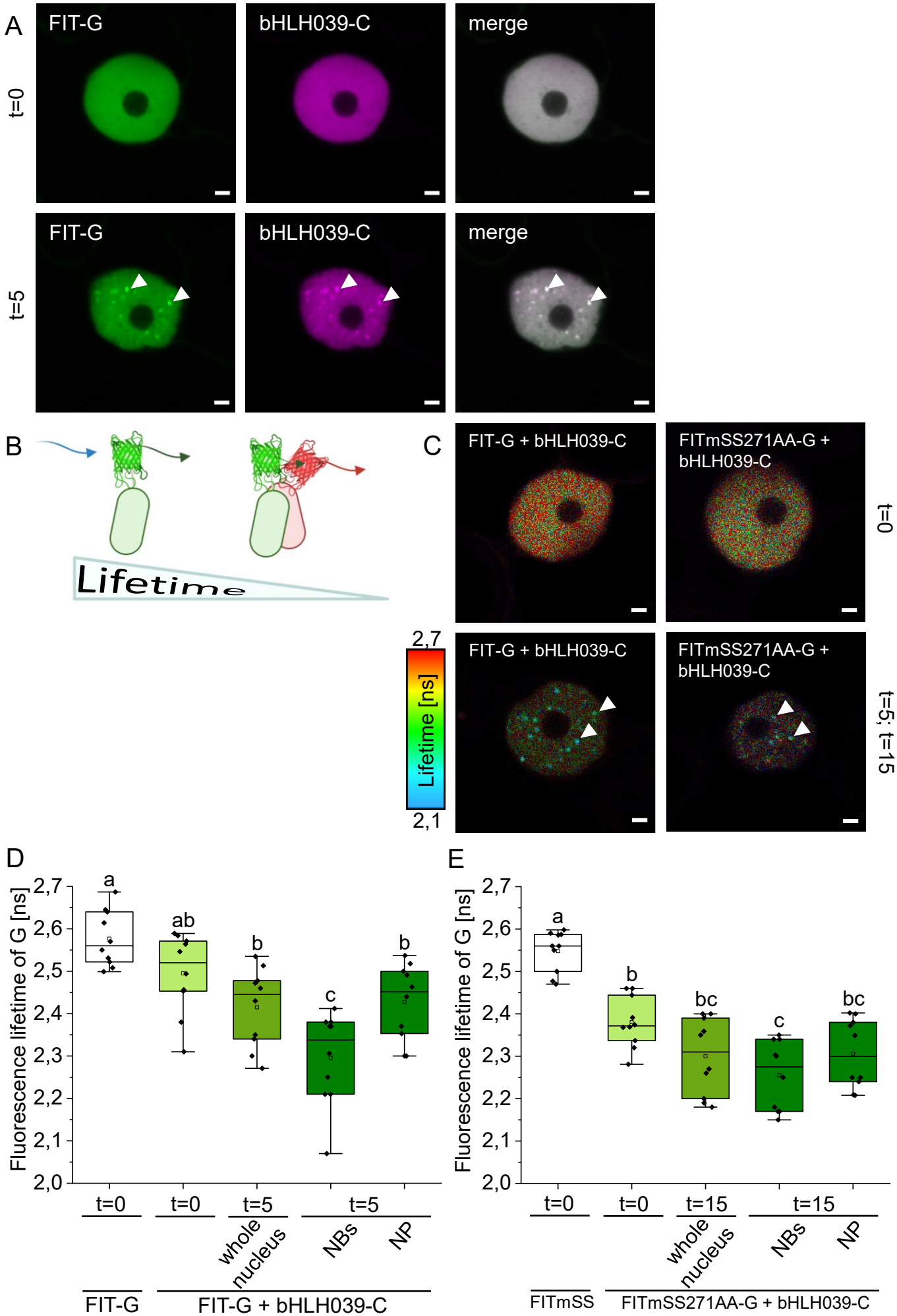
A
t=0
FIT-G
bHLH039-C
merge
t=5
FIT-G
bHLH039-C
merge
B
Lifetime
C
FIT-G + bHLH039-C
FITmSS271AA-G + bHLH039-C
t=0
2,7
Lifetime [ns]
2,1
FIT-G + bHLH039-C
FITmSS271AA-G + bHLH039-C
t=5; t=15
D
Fluorescence lifetime of G [ns]
2,7
2,6
2,5
2,4
2,3
2,2
2,1
2,0
a
ab
b
c
b
t=0
t=0
t=5
t=5
whole nucleus
NBs
NP
FIT-G
FIT-G + bHLH039-C
E
Fluorescence lifetime of G [ns]
2,7
2,6
2,5
2,4
2,3
2,2
2,1
2,0
a
b
bc
c
bc
t=0
t=0
t=15
t=15
whole nucleus
NBs
NP
FITmSS
FITmSS271AA-G + bHLH039-C

Figure 4: FIT was present in heterodimeric protein complexes with bHLH039 in NBs, dependent on Ser271/272 site.

A, Confocal images with colocalization of FIT-GFP and bHLH039-mCherry in the nucleus. Both proteins were evenly distributed within the nucleus at t=0 and colocalized fully in FIT NBs at t=5 min. Two independent experiments with two plants each. In all examined cells, the proteins showed full colocalization. Representative images from one nucleus. B-E, FRET-FLIM measurements to determine heterodimerization strength of FIT and FITmSS271AA with bHLH039, respectively. FIT-GFP and FITmSS271AA-GFP (donor only) served as negative controls. B, Schematic illustration of the FRET-FLIM principle. Energy transfer occurs between two different fluorophores. One fluorophore acts as the donor and the other as the acceptor of the energy. In case of interaction (close proximity, ≤10 nm) the fluorescence lifetime of the donor decreases. C, Representative images showing color-coded fluorescence lifetime values of FIT-GFP and FITmSS271AA-GFP co-expressed with bHLH039-mCherry at t=0 and t=5/15 min. D-E, Box plots diagrams representing FRET-FLIM measurements at t=0 within the whole nucleus and at t=5/15 min within the whole nucleus, inside NBs and in residual NP. Lifetime values represent measurements of 10 nuclei from a transformed plant (n = 10). Two experiments were conducted, one representative result is shown. Fluorescence lifetime was reduced for the pair of FIT-GFP and bHLH039-mCherry in NBs versus NP at t=5 min, indicating protein interaction preferentially inside NBs. Fluorescence lifetime values were not significantly different for the pair FITmSS271AA-GFP and bHLH039-mCherry in this same comparison at t=15 min, indicating that this pair did not preferentially interact in NBs. $IDR^{Ser271/272}$ may therefore be relevant for FIT NB formation, and FIT homo- and heterodimerization (**Supplemental Figure S2**).

Box plots show 25-75 percentile with min-max whiskers, mean as small square and median as line. Statistical analysis was performed with one-way ANOVA and Tukey post-hoc test. Different letters indicate statistically significant differences ($P < 0.05$). Scale bar: 2 µm. Arrowheads indicate NBs. G = GFP; C = mCherry. Fluorescence protein analysis was conducted in transiently transformed *N. benthamiana* leaf epidermis cells, following the standardized FIT NB analysis procedure.

Figure 5

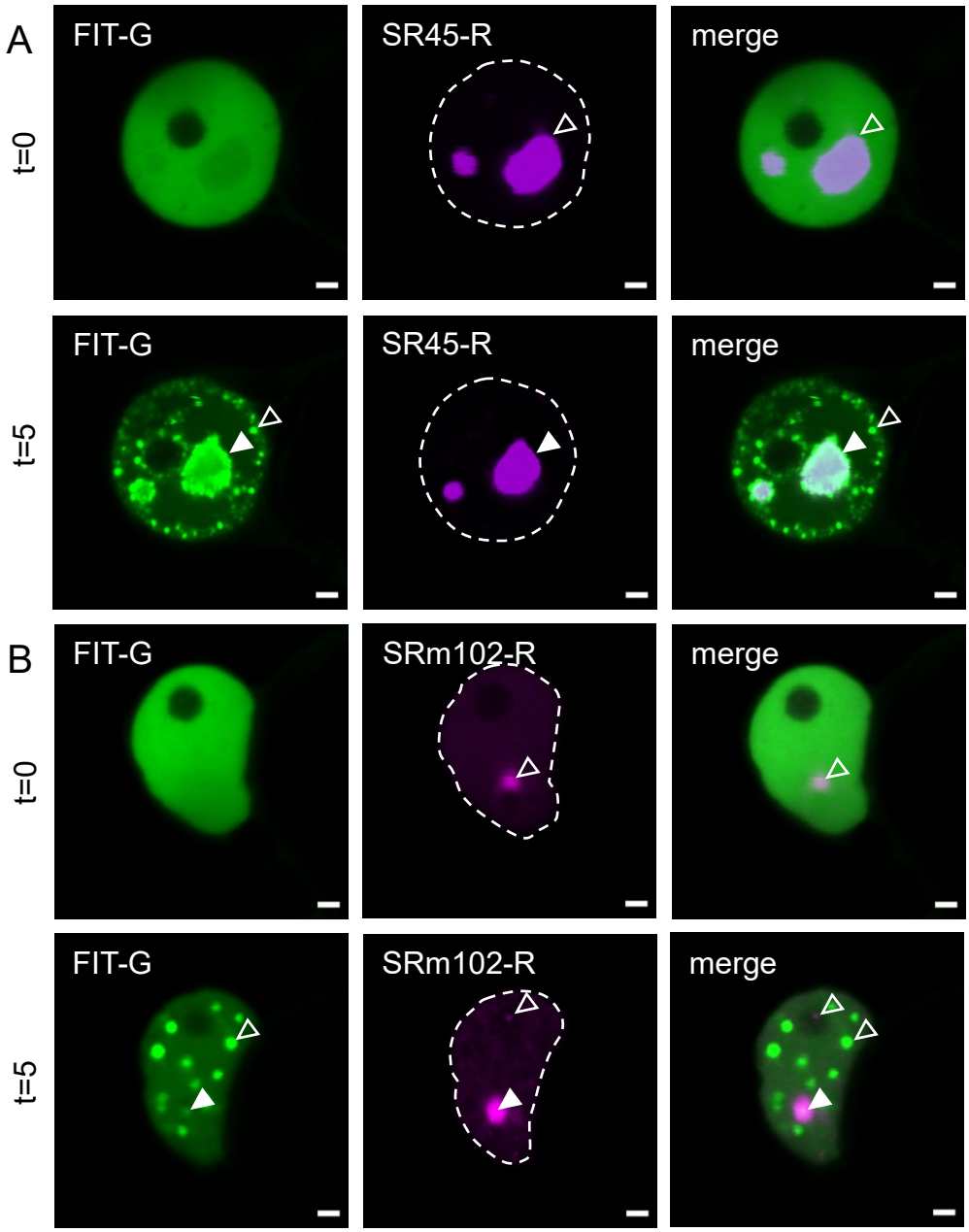

Figure 5: Two NB markers and splicing components were present in NBs (designated type II), revealing the dynamics of FIT to accumulate in NBs.

Confocal images showing localization of FIT-GFP and NB markers (type II) upon co-expression in the nucleus at t=0 and t=5 min. Co-expression of FIT-GFP with A, SR45-mRFP, and B, SRm102-mRFP. Type II NB markers localized inside NBs at t=0 and t=5 min. Similar localization patterns were observed upon single expression, showing that SR45 and SRm102 are present in distinct NB types (compare with **Supplemental Figure S4, A and B**). FIT-GFP colocalized with type II markers in their distinct NBs at t=5 min, but not t=0. FIT-GFP additionally localized in FIT NBs at t=5 min. Type II markers were not present in FIT NBs, while FIT-GFP became recruited into the distinct type II NBs upon the light trigger. Hence, FIT NBs could be associated with speckle components.

Scale bar: 2 µm. Filled arrowheads indicate colocalization in NBs, empty arrowheads indicate no colocalization in NBs. G = GFP; R = mRFP. Fluorescence protein analysis was conducted in transiently transformed *N. benthamiana* leaf epidermis cells, following the standardized FIT NB analysis procedure. In all examined cells, the proteins showed partial colocalization. Representative images from two to five independent experiments are shown. For data with type I markers (no colocalization) and type III markers (full colocalization) see **Supplemental Figure S3** and **Figure 6**.

Figure 6

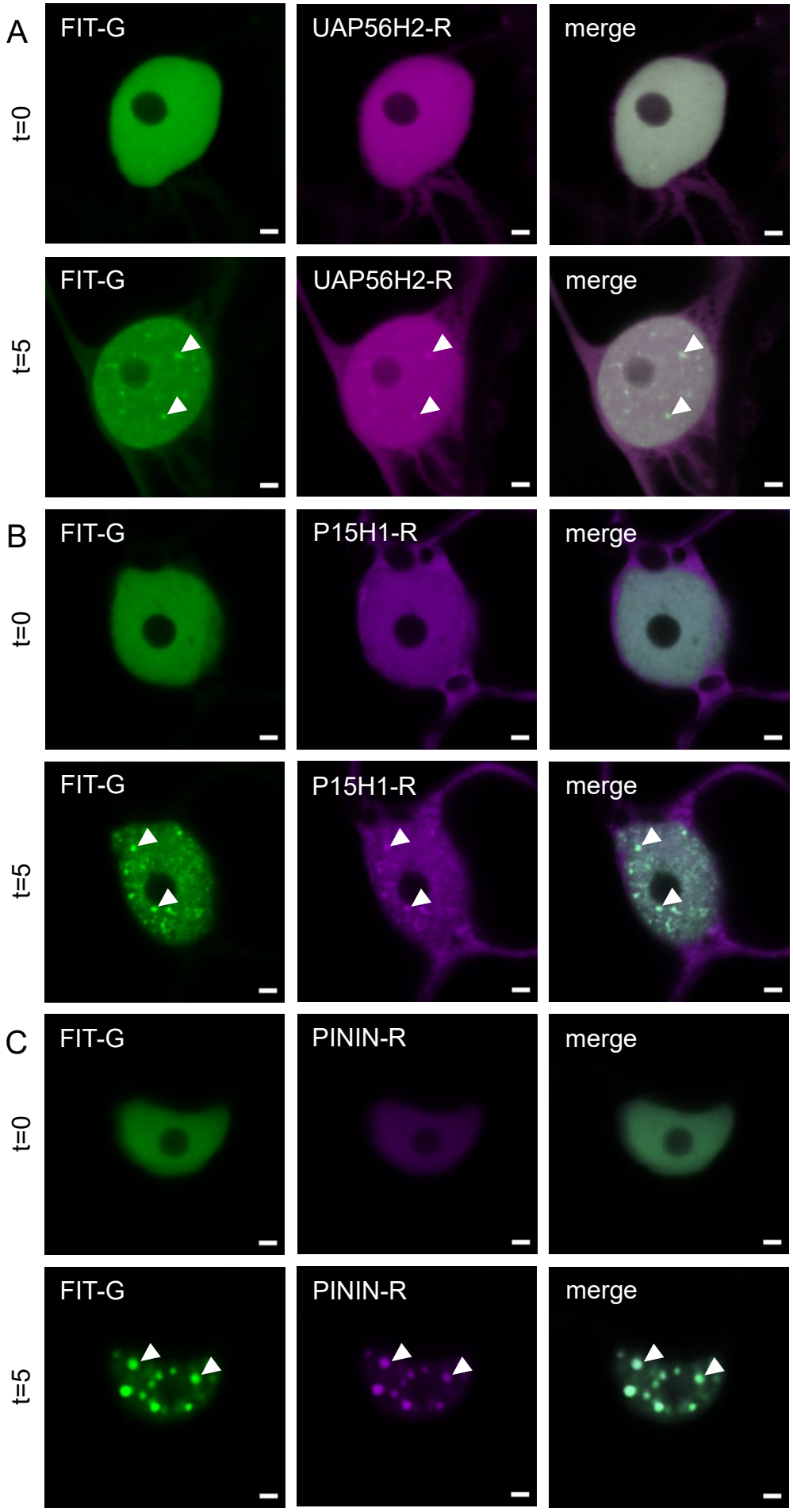
A
t=0
FIT-G
UAP56H2-R
merge
t=5
FIT-G
UAP56H2-R
merge
B
t=0
FIT-G
P15H1-R
merge
t=5
FIT-G
P15H1-R
merge
C
t=0
FIT-G
PININ-R
merge
t=5
FIT-G
PININ-R
merge

Figure 6: Three NB markers and speckle components became localized in FIT NBs and colocalized fully with FIT (designated type III), suggesting that FIT NBs have speckle function.

Confocal images showing localization of FIT-GFP and NB markers (type III) upon co-expression in the nucleus at t=0 and t=5 min. Co-expression of FIT-GFP with A, UAP56H2-mRFP, B, P15H1-mRFP, and C, PININ-mRFP. All three type III NB markers were homogeneously distributed and colocalized with FIT-GFP in the nucleus at t=0, while they colocalized with FIT-GFP in FIT NBs at t=5 min. UAP56H2-mRFP and P15H1-mRFP showed homogeneous localization in the single expression at both t=0 and t=5 min (compare with **Supplemental Figure S4, C and D**), while PININ-mRFP localized mainly in one large and several small NBs upon single expression at t=0 and t=5 min (compare with **Supplemental Figure S4E**). Hence, these three markers adopted the localization of FIT-GFP upon co-expression and suggest that FIT NBs have a speckle function.

Scale bar: 2 μm. Arrowheads indicate colocalization within NBs. G = GFP; R = mRFP. Fluorescence protein analysis was conducted in transiently transformed *N. benthamiana* leaf epidermis cells, following the standardized FIT NB analysis procedure. In all examined cells, the proteins showed full colocalization. Representative images from four to seven independent experiments are shown. Contrast of images in A at t=5 was enhanced for better assessment. For data with type I markers (no colocalization) and type II markers (partial colocalization) see **Supplemental Figure S** and **Figure 5**.

Figure 7

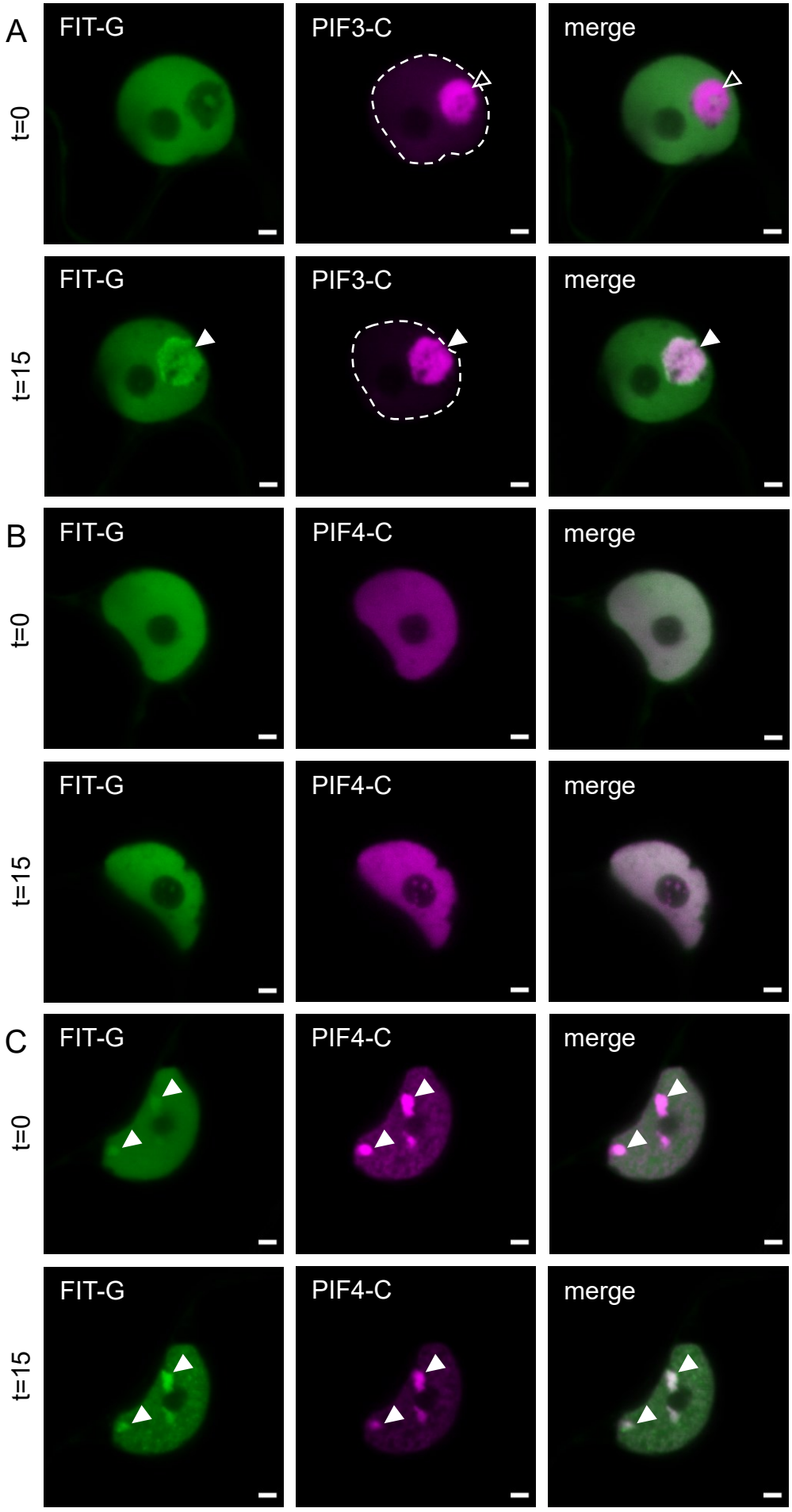
A
t=0
FIT-G
PIF3-C
merge
t=15
FIT-G
PIF3-C
merge
B
t=0
FIT-G
PIF4-C
merge
t=15
FIT-G
PIF4-C
merge
C
t=0
FIT-G
PIF4-C
merge
t=15
FIT-G
PIF4-C
merge

Figure 7: FIT colocalized with photobody (PB) markers in distinct PBs.

Confocal images showing localization of FIT-GFP and PB markers upon co-expression in the nucleus at t=0 and t=15 min. Co-expression of FIT-GFP with A, PIF3-mCherry, and B and C, PIF4-mCherry, in B, showing a typical pattern with absence of NBs (ca. 50% of nuclei), in C, showing a typical pattern with presence of NBs (ca. 50% of cells). When FIT-GFP was co-expressed with PB markers, FIT NBs did not appear at t=5 min, but instead, FIT-GFP colocalized with PB markers in PBs at t=15 min. A, PIF3-mCherry localized predominantly to a single large PB at t=0 and t=15 min. FIT-GFP colocalized with PIF3-mCherry in this single large PB at t=15 min. B, PIF4-mCherry and FIT-GFP were both homogeneously distributed in the nucleoplasm at t=0 and t=15 min. In C, FIT-GFP colocalized with PIF4-mCherry in PBs at t=0 and t=15 min. The same localization patterns were found for PIF3-mCherry and PIF4-mCherry upon single expression (compare with **Supplemental Figure S5**). Hence, FIT-GFP was recruited to the two distinct types of PIF3 and PIF4 PBs, whereas PIF3 and PIF4 were not recruited to FIT NBs. This suggests that FIT NBs are affected by the presence of PIF3- and PIF4-containing PBs and a connection to light signaling exists.

Scale bar: 2 µm. Arrowheads indicate colocalization in PBs. G = GFP; C = mCherry. Fluorescence protein analysis was conducted in transiently transformed *N. benthamiana* leaf epidermis cells, following the standardized FIT NB analysis procedure. In all examined cells, PIF3 and FIT colocalized fully, while PIF4 and FIT colocalized as indicated in B and C. Representative images from four to six independent experiments are shown.

Figure 8

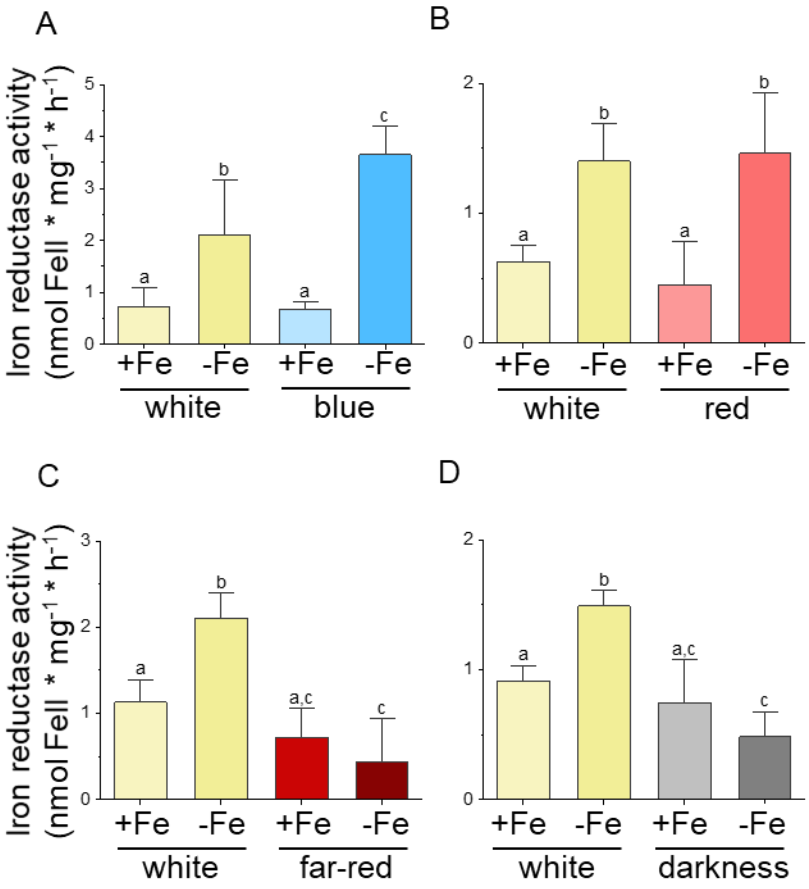
A
B
C
D
Iron reductase activity
(nmol FeII * mg-1 * h-1)
+Fe
-Fe
white
blue
red
far-red
darkness
a
b
c
a,c

Figure 8. Root iron reductase activity is promoted under blue light.

Root iron reductase activity assay on 6-d-old Arabidopsis seedlings grown under white light for 5 d under iron deficient and iron sufficient conditions and then exposed for 1 d to blue, red, far-red light or darkness, or in parallel as control to white light. A, Induction of iron reductase activity upon iron deficiency versus sufficiency was higher under blue light than compared to the white light control. B, Exposure to red light did not change the iron reductase activity compared to the white light control. C-D, Plants exposed to far-red light and darkness did not show induction of iron reductase activity under iron deficient conditions compared to the iron deficient conditions.

Two experiments were conducted, one representative result is shown. Bar diagrams represent the mean and standard deviation of four replicates with four seedlings each (n=4). Statistical analysis was performed with one-way ANOVA and Tukey post-hoc test. Different letters indicate statistically significant differences ($P < 0.05$).

Figure 9

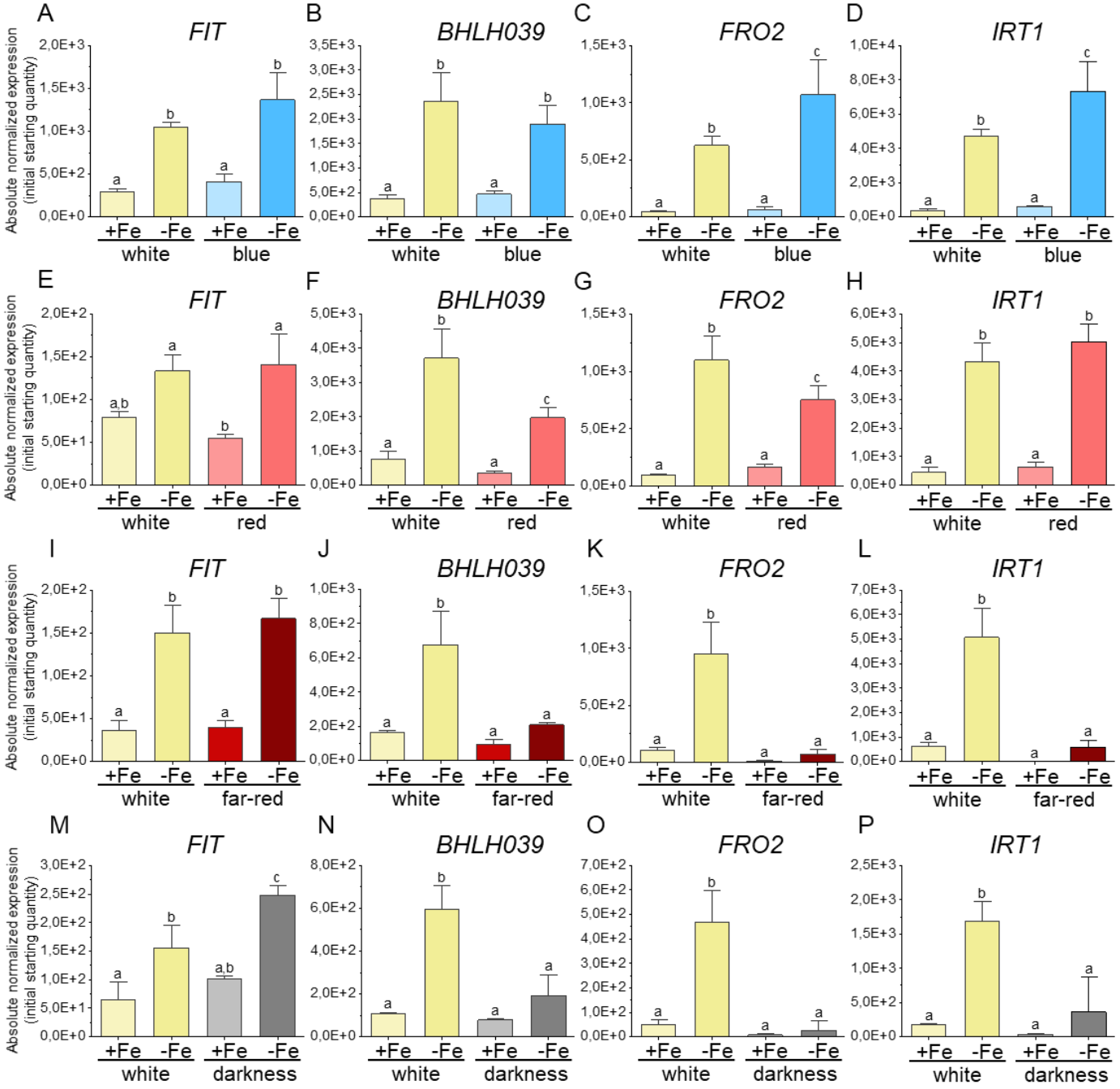
A
FIT
B
BHLH039
C
FRO2
D
IRT1
E
FIT
F
BHLH039
G
FRO2
H
IRT1
I
FIT
J
BHLH039
K
FRO2
L
IRT1
M
FIT
N
BHLH039
O
FRO2
P
IRT1
Absolute normalized expression
(initial starting quantity)
+Fe
-Fe
white
blue
red
far-red
darkness

Figure 9. Induction of FIT target gene expression is enhanced under blue light.

Gene expression analysis of iron deficiency genes *FIT*, *BHLH039*, *FRO2*, and *IRT1* on 6-d-old Arabidopsis seedlings grown under white light for 5 d under iron deficient and iron sufficient conditions and then exposed for 1 d to blue, red, far-red light or darkness, or in parallel as control to white light. A-B, *FIT* and *bHLH039* gene induction in response to low iron supply did not change after blue light exposure compared to the white light control. C-D, *FRO2* and *IRT1* gene expression increased after blue light exposure in iron deficient conditions compared to respective iron sufficient condition and white light control. E, *FIT* gene expression did not change after red light exposure compared to the white light control. F-G, *BHLH039* and *FRO2* gene expression decreased after red light exposure in iron deficient conditions compared to respective iron sufficient condition and white light control. H, *IRT1* gene expression did not change after red light exposure compared to the white light control. I, *FIT* gene expression did not change after far-red light exposure compared to the white light control. J-L, *BHLH039*, *FRO2*, and *IRT1* gene expression decreased after far-red light exposure in iron deficient conditions compared to white light deficient condition, comparable to the respective iron sufficient condition and iron sufficient white light control. M, *FIT* gene expression was higher in darkness under iron deficient conditions compared to respective iron sufficient condition and white light control. N-P, *BHLH039*, *FRO2*, and *IRT1* gene expression decreased after being exposed to darkness in iron deficient conditions compared to white light deficient condition, comparable to the respective iron sufficient condition and iron sufficient white light control.

Two experiments were conducted, one representative result is shown. Bar diagrams represent the mean and standard deviation of three replicates with twelve seedlings and two technical replicates each (n=3). Statistical analysis was performed with one-way ANOVA and Tukey post-hoc test. Different letters indicate statistically significant differences ($P < 0.05$).

Figure 10

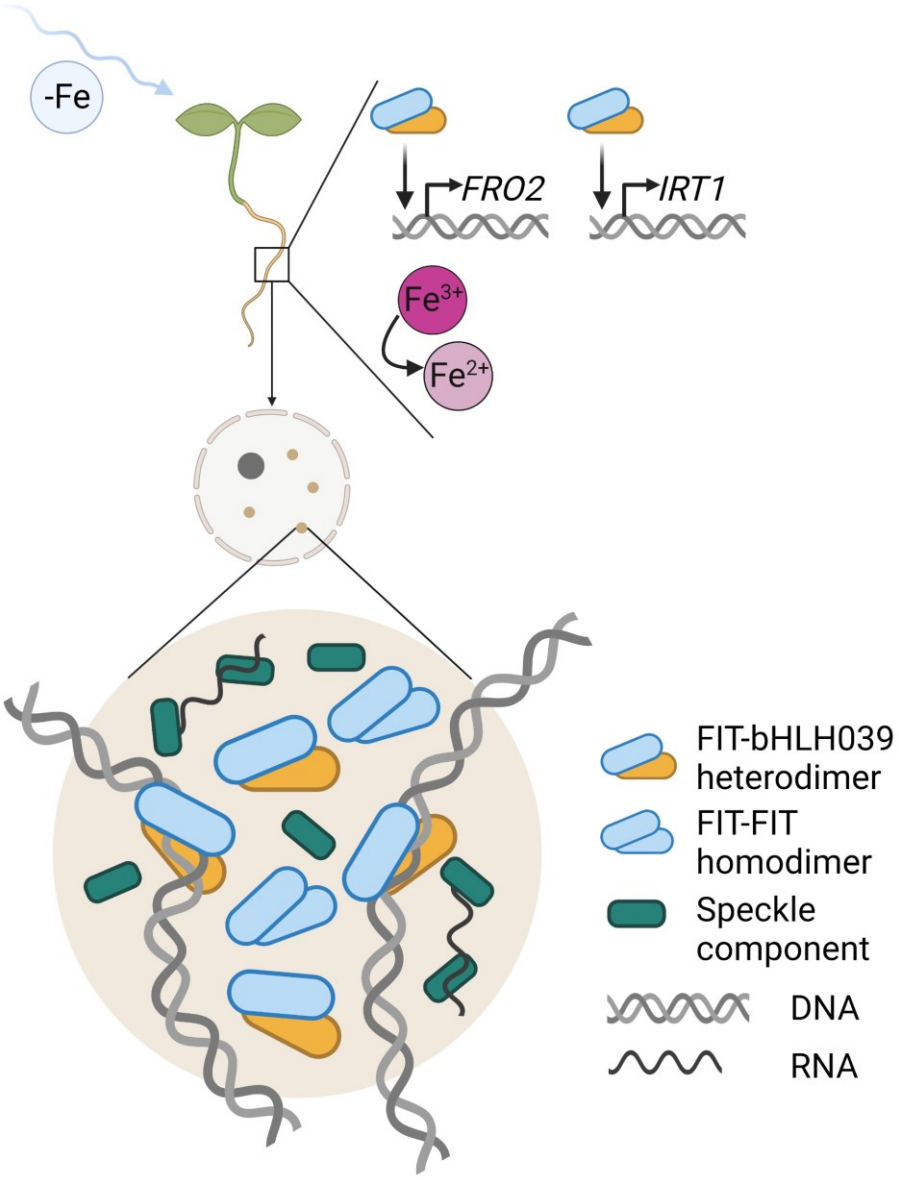
-Fe
FRO2
IRT1
Fe3+
Fe2+
FIT-bHLH039 heterodimer
FIT-FIT homodimer
Speckle component
DNA
RNA

Figure 10: Summary model illustrating the effect of blue light on FIT NB formation and iron uptake, suggesting that FIT NBs are related to transcriptional and posttranscriptional regulation in speckles and that blue light has a promoting effect on iron uptake.

FIT accumulates in FIT NBs upon induction with blue light. FIT NBs are reversible, dynamic and of circular shape and may undergo LLPS. FIT homodimers and FIT-bHLH039 heterodimers are present in FIT NBs. FIT-bHLH039 is an active TF complex for upregulating the expression of iron acquisition genes in roots (Gratz et al., 2019). Hence, FIT NBs are subnuclear sites related to transcriptional regulation and because of their colocalization with speckle components, also to speckles. Blue light enhances root iron reductase activity and gene expression of *FRO2* and *IRT1*, all of which are downstream of FIT-bHLH039. In summary, FIT NBs are blue light-inducible subnuclear sites where active TF complexes of FIT and bHLH039 accumulate, linking transcriptional and posttranscriptional regulation in speckles with a promoting blue light effect on iron uptake.